α7 nicotinic acetylcholine receptors regulate radial glia fate in the developing human cortex

Tanzila Mukhtar[1,2,#,*], Clara-Vita Siebert[1,2,3,*], Yuejun Wang[1,2,*], Mark-Phillip Pebworth[1,2,4,*], Matthew L. White[1,2], Tianzhi Wu[1,2], Tan Ieng Huang[1,2], Guolong Zuo[1,2], Jayden Ross[1,2], Jennifer Baltazar[1,2], Varun Upadhyay[1,2], Merut Shankar[1,2], Li Zhou[1,2], Isabel Lombardi-Coronel[1,2], Ishaan Mandala[1,2], Manal A. Adam[1,2], Shaohui Wang[1,2], Qiuli Bi[1,2], Marco F.M. Hoekman[3], Jingjing Li[1,2] and Arnold R. Kriegstein[1,2,#]

1. Department of Neurology, University of California, San Francisco (UCSF), San Francisco, CA, USA, 94143
2. The Eli and Edythe Broad Center of Regeneration Medicine and Stem Cell Research, UCSF, San Francisco, CA, USA, 94143
3. Swammerdam Institute for Life Sciences, University of Amsterdam, 1098 XH Amsterdam, The Netherlands
4. Allen Institute of Immunology, Seattle, WA 98109

*These authors contributed equally

#Correspondence should be addressed to Tanzila.mukhtar@ucsf.edu and Arnold.Kriegstein@ucsf.edu

Abstract

Prenatal nicotine exposure impairs fetal cortical grey matter volume, but the precise cellular mechanisms remain poorly understood. This study elucidates the role of nicotinic acetylcholine receptors (nAChRs) in progenitor cells and radial glia (RG) during human cortical development. We identify two nAChR subunits—CHRNA7 and the human-specific CHRFAM7A—expressed in SOX2+ progenitors and neurons, with CHRFAM7A particularly enriched along RG endfeet. nAChR activation in organotypic slices and dissociated cultures increases RG proliferation while decreasing neuronal differentiation, whereas nAChR knockdown reduces RG and increases neurons. Single-cell RNA sequencing reveals that nicotine exposure downregulates key genes in excitatory neurons (ENs), with CHRNA7 or CHRFAM7A selectively modulating these changes, suggesting an evolutionary divergence in regulatory pathways. Furthermore, we identify YAP1 as a critical downstream effector of nAChR signaling, and inhibiting YAP1 reverses nicotine-induced phenotypic alterations in oRG cells, highlighting its role in nicotine-induced neurodevelopmental pathophysiology.

Introduction

Neurodevelopmental and neuropsychiatric diseases including autism, schizophrenia, and attention deficit hyperactivity disorder (ADHD) have been linked to maternal smoking during pregnancy[1-3].

Despite the risks to fetal development, a global average of 1.7 - 21% of pregnant mothers continue to smoke[4,5]. Not only are the by-products of cigarette smoke harmful, but the active compound nicotine poses significant risks, raising concern about the safety of nicotine replacement therapy during pregnancy[6,7]. Nicotine, an exogenous ligand of nicotinic acetylcholine receptors (nAChRs), competes with the endogenous neurotransmitter acetylcholine (ACh). Notably, nicotine exhibits a higher binding affinity for nAChRs than ACh, potentially amplifying its impact on the developing brain[8]. Evidence suggests that prenatal smoking or smokeless nicotine exposure leads to reduced cortical grey matter volume, cortical thinning, and behavioral abnormalities in offspring[6,7,9-12]. The Generation R study that followed children of 113 mothers who smoked during pregnancy found behavioral abnormalities and changes in brain morphology by school-age[12]. Despite consistent pathological effects, the molecular mechanism by which smoking causes cortical and behavioral abnormalities remains elusive.

Nicotine exposure has a variety of effects on brain development in rodents and non-human primates that manifest in particular brain regions (including neocortex) and at specific developmental time points[13-16]. NAChRs are expressed in mice as early as embryonic day 10 (E10) when progenitor cells are the most prevalent cells in the cortex[17]. Moreover, most E10-E11 neurons show functional responses to the broad AChR agonist, ACh, as well as the more specific agonist, nicotine[17]. Rodent studies have shown that nicotine can affect neurogenesis and differentiation as well as synaptic development[18-21]. *In vivo* studies in rodents show an increase in adult SVZ neurogenesis upon nicotine exposure mediated by FGF2 signaling[22,23]. However, non-human primates, such as Rhesus monkeys, provide a closer approximation of human brain development than rodent models. Nicotine administered to pregnant Rhesus monkeys at plasma levels comparable to human smokers alters the expression of α4β2 and α7 nAChRs and impairs neurite formation in the cortex of their affected offspring[15]. Despite the diverse effects nicotine can have on animal models, consequences of nicotine exposure on early developing human cortex remain unclear.

NAChR receptors are pentameric ligand-gated ion channels formed from a combination of subunits including α2-7, 9, 10 that play crucial roles in neural maturation and synaptic transmission[13,24]. The α7 nAChR is formed as a homomeric pentamer of the α7 subunit that is encoded by the CHRNA7 gene. This receptor plays a crucial role in cognitive function and has been implicated in schizophrenia[13,25,26]. During evolution, a partial duplication of the CHRNA7 gene has led to the formation of the human-specific gene CHRFAM7A[24]. CHRFAM7A encodes for the peptide subunit dupa7 that assembles with the native α7 subunit[27,28]. Microdeletions in CHRNA7 and CHRFAM7A have been associated with schizophrenia and bipolar disorder[24,29,30]. Despite the importance of nAChRs in human cognition and

disease[27,28,31,32], the expression and roles of CHRNA7 and CHRFAM7A during human cortical development are not well understood.

Here we investigate the role of cholinergic signaling mediated through ACh or nicotine, and the role of CHRNA7 and CHRFAM7A in human radial glia (RG) and progenitor cells during cortical development. We use a range of model systems, including *ex vivo* organotypic slice cultures from primary developing human cortical samples, dissociated primary cortical cell cultures, and induced pluripotent stem cell (iPSC)-derived cerebral organoids.

Results

Cholinergic fibers and outer radial glia (oRG) colocalize in the developing human cortex

Cholinergic signaling in the developing cerebral cortex is largely mediated through cholinergic fibers from the nucleus basalis of Meynert, a cluster of cholinergic neurons in the basal forebrain[33], that innervate the cerebral cortex and express choline acetyltransferase (ChAT) and acetylcholinesterase (AChE)[34,35]. In humans, cholinergic fibers project towards the cerebral cortex as early as gestational week 12 (GW12)[34]. We sought to characterize the cortical location of cholinergic fibers relative to the RG-rich germinal zone (GZ). RG residing along the lateral ventricles are the principal stem cells of the developing human cortex, giving rise to oRG cells, intermediate progenitor cells (IPCs), neurons, and glia[36]. Humans have large numbers of oRG cells compared to mice, and they are thought to serve as key drivers of the expansion of the neocortex, particularly contributing to upper layer neurons[36,37]. We performed co-immunostaining for AChE, HOPX (a marker of oRG cells), and Vimentin (VIM, a marker of RG and oRG fibers), in coronal sections of primary developing human prefrontal cortex at GW15, and GW22 (Fig.1a). AChE was enriched in the outer subventricular zone (oSVZ), cortical plate (CP), and marginal zone (MZ), and colocalized with HOPX+ oRG cells and VIM+ radial fibers (Fig.1b). We also observed similar patterns of AChE expression in GW15 and GW22 motor cortex and visual cortex (Extended Data Fig.1a,b). These similar patterns across different cortical areas suggest a pervasive role of cholinergic signaling during cortical development.

CHRNA7 and CHRFAM7A receptor subunits are expressed in major cortical progenitor niches

We hypothesized that due to the co-localization of AChE+ fibers and oRG cells, that ACh might functionally interact with oRG cells in the oSVZ progenitor niche. To investigate the cell types potentially responsive to cholinergic signals, we used a single-cell RNA-seq (scRNAseq) dataset of developing human cortex (hgwdev-max.soe.ucsc.edu/tsneViewer/dev3/) and verified the RNA expression of four nAChRs subunits: CHRNA7; CHRFAM7A; CHRNB1; and CHRNB2. All four subunits, though mostly

studied in neurons, were also expressed by RG, dividing progenitors, and oRG cells, as well as early neurons, with CHRNA7 and CHRFAM7A showing more abundant expression in progenitors than CHRNB1 and CHRNB2 (Extended Data Fig.2a). To validate translation of RNA into functional receptors, we performed Western blotting on protein lysates isolated from either whole cortices or the GZ of primary developing tissue obtained by microdissection. We collected two or three biological replicates per preparation type, spanning periods of high neurogenesis (GW15-GW19) and gliogenesis (GW20-GW23). We observed protein expression of CHRNA7, CHRFAM7A, CHRNB1 and CHRNB2 across all time points in whole cortex lysates and enriched GZ samples (Extended Data Fig.2c-e).

To further validate cell-type-specific receptor expression in primary cortical sections (GW17-23), we performed RNAscope (for CHRNA7) and BaseScope (for CHRFAM7A) and co-immunostained for the progenitor cell marker, SOX2 (Fig.2a)[38]. We observed high expression of CHRNA7 in the ventricular zone (VZ) and CP, and colocalization with both SOX2+ and SOX2- cells indicating broad expression in different cell types (Fig.2a). CHRFAM7A RNA was highly expressed in the apical endfeet of RG and in the CP at GW17 (Fig.2a''). Both subunits were expressed in SOX2+ oRG cells (Fig.2b,c)[37]. Immunostaining for CHRNA7 and CHRFAM7A also validated protein expression of these subunits in SOX2+ progenitors within the VZ and in NEUN-expressing neurons in the CP, with lower expression in the oSVZ (Fig.2b,c and Extended Data Fig. 3). Expression was also observed in ZO-1+ RG apical endfeet contacting the ventricle (Extended Data Fig.2b), an expression pattern that might indicate a role for cholinergic signaling mediated by CSF. Choline is a selective activator of α7 nAChRs, that have lower affinities than other nAChRs for nicotine and ACh[13,39]. Choline is present in high concentrations in the developing fetus and is a source of cholinergic signaling during human cortical development[40,41]. These results indicate that RG and oRG cells express a variety of specific nAChRs.

IPSC-derived cortical organoids display nAChR expression patterns observed in primary tissue

To further study the observed expression patterns of CHRNA7 and CHRFAM7A in neuronal lineage cells, we utilized iPSC-derived cortical organoids. Cortical organoids are 3D spheres derived from pluripotent stem cells through the addition of morphogens and growth factors that mimic *in vivo* developmental signals[42,43]. We found CHRNA7 and CHRFAM7A protein expressed in organoids across a developmental time-course corresponding to progenitor expansion (week four), early neurogenesis (week seven), peak neurogenesis (week nine) and early gliogenesis (week 13) (Extended Data Fig.2f)[44]. Comparable to primary tissue, we observed high CHRFAM7A expression in KI67+ cells in the progenitor-rich neural rosettes, including along the apical border, at weeks 7-9 (Fig.2d, d'). By weeks 13-15 we observed the expression of CHRFAM7A in SOX2+ and NEUN+ cells (Fig.2e). Thus, cortical

organoids have similar expression patterns for CHRNA7 and CHRFAM7A as primary tissue and are a reasonable model system to investigate cholinergic signaling.

Activation of nAChRs promotes the proliferation of progenitors while reducing the number of neurons in the developing human cortex.

To investigate the functional implications of cholinergic signaling, we treated organotypic cortical slice cultures at GW18-19 (n=3) with two broad nAChR agonists; acetylcholine and nicotine, and included an EdU pulse 24 hr before fixation (Fig.3a). Upon ACh or nicotine treatment, the number of SOX2+ progenitors increased significantly compared to untreated (UT) control (Fig.3b,c). Likewise, KI67+ proliferating cells increased in ACh and nicotine conditions (Fig.4b,c), consistent with an observed increase in EdU-positive cells (Fig.3b,c). EOMES+ intermediate progenitor cells (IPCs) increased post nicotine treatment, while remaining unchanged after ACh, suggesting different responses to ACh and nicotine (Fig.3d,e). Nicotine primarily targets nAChRs, whereas ACh interacts with both nicotinic and muscarinic acetylcholine receptors[45]. Additionally, we observed a significant increase in HOPX+ oRG cells in both conditions compared to controls (Extended Data Fig.4a,b). The balance between progenitor self-renewal and neuronal differentiation is tightly regulated in the developing cortex[36]. During the second trimester (GW15-19), RG and oRG cells generate large numbers of cortical neurons[36]. We investigated if the increased self-renewal of RG, oRG, and IPCs impacts neuronal differentiation. We found an increase in double-positive KI67 and EdU cells following ACh and nicotine treatment, indicating extended cell cycle length (Extended Data Fig.4a,b). Indeed, the increase in progenitor cells was associated with a reduction in NEUN+ neurons affecting both deep (CTIP2+) and upper (SATB2+) layer neurons (Fig.3d, Extended Data Fig.4a,a',b). The NEUN+ neurons were reduced with ACh and nicotine, impacting deep layer CTIP2+ neurons in the IZ. To investigate the impact of ACh and nicotine on gliogenesis, we quantified astrocytes (labeled with S100B) and oligodendrocytes (labeled with OLIG2) (Extended Data Figures 4c and 4d). We found no significant changes in S100B and OLIG2 expression during the 5-day chase after agonist treatment. However, previous studies have observed changes in astrocytes and oligodendrocytes following nicotine exposure, possibly attributed to different exposure paradigms used[46,47]. We also observed no significant change in DLX5 interneurons or cell death across conditions (Extended Data Fig.4e,f). While we assessed DLX5-positive cells in the cortex, we did not investigate the effects of nicotine exposure on the ganglionic eminence, which is the primary source of cortical interneurons.

To validate the role of the α7 nAChR in these phenotypic changes, we treated organotypic slices with a highly specific agonist, PNU, and included DMSO as a negative control. We observed that PNU was

171 sufficient to increase SOX2+, HOPX+, and KI67+ progenitors (Fig.3e,f, Extended Data Fig.4g,h). PNU
172 increased SOX2+ cells, but did not reach statistical significance (p= 0.054). HOPX+ and KI67+ cells
173 increased post PNU treatment. PNU did not significantly impact EOMES+ IPCs or EdU incorporation
174 (Fig.3e,f and Extended Data Fig.4g,h). This suggests the α7 nAChR is involved in neurogenesis
175 through activation of HOPX+ oRG cells. We observed a reduction in NEUN+ neurons with PNU,
176 impacting CTIP2+ deep layer neurons, with no change in upper layer SATB2+ neurons (Fig.3e and
177 Extended Data Fig.4h,i). DLX5 interneurons did not change in number and there was no increase in cell
178 death (Extended Data Fig.4j,k). Overall, these results show that broad activation of nAChRs through
179 ACh or nicotine promotes progenitor cell fate at the cost of neurogenesis. Activation of the α7 nAChR
180 recapitulates several of the phenotypic features observed with ACh or nicotine exposure, confirming a
181 role of the α7 nAChR in progenitor maintenance, proliferation, and regulation of neurogenesis in
182 developing human cortex.
183
184 ***Activation of nAChRs in cortical organoids partially phenocopies activation in primary tissue***
185 Cortical organoids provide a useful model system to manipulate signaling effectors. To replicate our
186 observations from primary tissue, we treated cortical organoids derived from three iPSC lines (H1,
187 1323-4 and WTC-11) with ACh, nicotine or PNU after seven weeks of differentiation, a time-point
188 corresponding to a period of neurogenesis[44] (Fig.4a). We observed a significant increase in SOX2+
189 progenitors with both ACh and nicotine and a simultaneous reduction in NEUN+ neurons (Fig.4b-d).
190 Specifically, SATB2+ upper layer neurons decreased in both conditions, while the number of CTIP2+
191 deep layer neurons was reduced in nicotine treated organoid cultures only (Fig.4b-d). We observed a
192 trend toward an increase of SOX2+ progenitors and a reduction in NEUN+ cells in PNU treated
193 organoids (Fig.4e-f).
194
195 The generation of deep-layer CTIP2+ neurons in organoids starts at stages prior to seven weeks, and
196 the absence of changes in CTIP2+ neurons in ACh treated organoids might be due to the
197 developmental window when the organoids were treated[42]. To test the impact of AChR agonists on
198 CTIP2+ deep-layer neurons, we treated cortical organoids derived from three different cell lines at a
199 younger age (week 5) for four days (Extended Data Fig.5a). We observed a consistent increase in
200 SOX2+ progenitors with ACh and nicotine (Extended Data Fig.5a-c) accompanied by a simultaneous
201 reduction in NEUN+ and CTIP2+ cells (Extended Data Fig. 5a-c).
202
203 We attempted to rescue the phenotypes by adding the α7 nAChR antagonist, α-Bungarotoxin (BTX)[48].
204 There were no phenotypic changes in progenitors or neurons with BTX, but in combination with the

agonists (ACh or nicotine), BTX was able to normalize the percentages of SOX2+, NEUN+ and CTIP2+ cells (Extended Fig.5b). We observed significant changes in NEUN+ cells, compared to UT controls. CTIP2+ cells changed slightly. This rescue suggests that blocking the α7 nAChR receptor can at least partially reverse the observed agonist-mediated phenotypic changes, and activation of β-receptors may partially explain the incomplete rescue. Thus, the observed effects are likely mediated, in part, by the α7 nAChR. We also tested PNU in early cortical organoids but did not observe a significant phenotype in progenitors or neurons, suggesting potential mechanistic differences between early and late neurogenic organoids downstream of agonist treatment (Extended Data Fig.5d,e). We noticed no changes in oRG cells in the presence of agonist (Extended Data Fig.5f), although there are very few HOPX+ oRG cells at this stage[44]. These observations highlight that broad activation of nAChRs in early organoids recapitulates several phenotypic changes in fetal progenitors, and can impact CTIP2+ early born deep-layer neurons. Temporal patterning and cell fate decisions are critical during cortical development and nAChRs appear to regulate these fundamental processes.

Loss-of-function of CHRNA7 and CHRFAM7A show inverse phenotypic changes compared to receptor activation

We conducted loss-of-function experiments to further test the role of nAChRs during cortical development. Lentiviral vectors expressing shRNAs and RFP were used to infect dissociated primary cortical cultures derived from GW14–18 tissue samples (n=4) (Extended Data Fig.6a). Using RT-qPCR, we observed a 43% and 54% reduction in mRNA expression of the respective subunits in shCHRNA7 and shCHRFAM7A treated cultures compared to scrambled controls (shCONTROL) (Extended Data Fig.6b). We also tested the lentiviral infection efficiency in organotypic slices and observed a comparable number of RFP+ cells across conditions (Extended Data Fig.6b).

We treated organotypic slice cultures (GW15, 17 and 21, n=3) with shRNAs for seven days and used immunostaining to analyze potential phenotypic changes (Fig.5a). We observed a reduction of SOX2+ progenitors upon loss-of-function of CHRNA7 and CHRFAM7A, an effect opposite to agonist treatment (Fig.3b,c). We also observed a reduction in KI67+ dividing progenitors (Fig.5b-d). We found no change in EOMES+ IPCs (Fig.5c,e). The number of NEUROD1+ newborn neurons, increased upon knockdown of CHRFAM7A while NEUN+ neurons increased upon knockdown of both CHRNA7 and CHRFAM7A (Fig.5c,e). To investigate the role of nAChRs in gliogenesis, we performed immunostaining for S100B and OLIG2, markers of astrocytes and oligodendrocytes, respectively. We found a reduction in astrocytes and a significant decrease in oligodendrocytes (Fig. 5c,f). Our findings suggest that both CHRNA7 and CHRFAM7A subunits are required for RG maintenance, proliferation and gliogenesis.

239 The human specific CHRFAM7A appears to play a critical role in neurogenesis, consistent with its high
240 expression in ventricular RG.
241
242 ***RNA sequencing reveals the molecular changes associated with nAChR signaling***
243 To derive a mechanistic understanding about cholinergic signaling in progenitor cells, we performed
244 bulk RNA-sequencing following nAChR knockdown. We microdissected the GZ from GW15-23 cortical
245 slice cultures (n=4, biological replicates). Since choline is present at high concentrations in the
246 developing fetal brain[13,39,41], we hypothesized that treatment with shRNAs against CHRNA7 or
247 CHRFAM7A would allow us to explore loss-of-function of nAChRs (Extended Data Fig.6a,b).
248 Knockdown of CHRNA7 upregulated CACNA1A, a gene involved in neurogenesis and implicated in
249 autism spectrum disorder (ASD) and epileptic encephalopathy[49] (Extended Data Fig.6c). We also found
250 upregulation of UNC5C, known to be involved in axon extension and migration[50,51]. CHRNA7 loss
251 upregulated GABRG3, a gene mediating neuronal inhibition that has been associated with ASD[52].
252 CHRNA7 knockdown caused a downregulation of GNB1, which is a heterotrimeric G-protein that
253 integrates signals between receptors and effector proteins. GNB1 is associated with Global
254 Developmental Delay, a disorder characterized by intellectual disability and seizures[53]. Knockdown of
255 CHRNA7 also caused a reduction in PSAT1, a gene whose expression is reduced in schizophrenia[54].
256 To identify which biological processes are most affected by knockdown of CHRNA7, we conducted GO
257 analysis and found basic processes such as semaphorin receptor signaling, chemokine receptor
258 binding, and STAT pathway among upregulated processes. We also observed downregulation of
259 glycerolipid metabolism, phospholipid metabolism, and acetylcholine-gated cation channel activity,
260 consistent with CHRNA7 regulating a variety of basic cellular processes in cortical progenitors
261 (Extended Data Fig.6d).
262
263 We observed downregulation of multiple genes upon knockdown of CHRFAM7A, including PPP1CA,
264 IL6ST, CALR, and RCN2 (Extended Data Fig.6c). IL6ST, highly enriched in neural progenitors, is a
265 signal transducer shared by various cytokines including LIF. LIF signaling has recently been shown to
266 regulate the production of cortical interneurons by oRG cells[55]. CALR is a chaperone protein involved in
267 a variety of cellular processes including protein folding and calcium homeostasis, and CALR release
268 recruits and activates microglia[56,57]. RCN2 (TCBP49) is a calcium-binding protein in the endoplasmic
269 reticulum (ER), expressed in neurons and glia[58]. We also found that downregulated biological
270 processes post CHRFAM7A knockdown included metabolic processes involving Oncostatin, LIFR,
271 tyrosine kinase, and Wnt pathways (Extended Data Fig.6e,f). We validated downstream targets of
272 CHRNA7 and CHRFAM7A by RT-qPCR and found similar up or downregulation of UNC5C, BMP2,

273 TKTL1, CXCL10, and HTR2A (Extended Data Fig.6g) as observed in bulk RNA (Extended datasheet
274 2). BMP2 encodes a TGF-β receptor ligand and is involved in critical developmental processes,
275 including neurogenesis[59]. TKTL1 belongs to the transketolase family of enzymes and is preferentially
276 expressed in neural progenitors[60]. A lysine-to-arginine substitution present in the modern human TKTL1
277 gene, but not present in the Neanderthal version, has been reported to increase the number of oRG
278 cells in prenatal cortex and the neurons they produce[60]. CXCL10 is secreted by neurons and astrocytes
279 and plays an essential role in cell migration[61-64]. HTR2A encodes a serotonin receptor expressed in RG,
280 and mutations in this gene are associated with neuropsychiatric disorders including major depressive
281 disorder and obsessive-compulsive disorder[65-67].
282
283 Comparing CHRNA7 and CHRFAM7A knockdown, we found shared candidates including CIR1,
284 FBXL16, NHSL1 among upregulated and AK4P3, GSTM5, SCN1A among downregulated genes.
285 (Extended Data Fig.6h). Intriguingly, twice as many genes were differentially expressed between
286 CHRNA7 and CHRFAM7A knockdown (Extended Data Fig.6h, Extended datasheet 2), suggesting that
287 CHRNA7 and CHRFAM7A may mediate different downstream pathways in cortical cells. Our data
288 highlight gene targets of nAChRs in the progenitor rich germinal zones of developing human cortex,
289 including several genes that are implicated in neurodevelopmental and behavioral disorders.
290
291 ***Cell type specific differential gene expression following nicotine exposure***
292 To better elucidate the effects of nicotine exposure and nAChR subunit loss-of-function on specific cell
293 types, we performed scRNAseq (Fig.6a). We used dissociated primary cultures derived from second
294 trimester tissue samples and treated them with nicotine to simulate nicotine exposure or performed
295 shRNA-mediated knockdown of nAChRs (Fig.6a). We examined two age groups, GW15-GW16 and
296 GW19-22 and performed scRNAseq of 19,661 cells that passed quality control. GW15-GW16
297 corresponds to peak neurogenesis, while gliogenesis is ongoing at GW19-22[68]. Samples from GW15-
298 16 will be referred to as neurogenic, while samples from GW19-22 will be referred to as gliogenic. Each
299 sample showed a consistent distribution of known cortical cell types across ages (Extended Data
300 Fig.7a,b). UMAP clustering resolved the data into 25 clusters, capturing all major cortical cell types and
301 samples (Fig.6b,c, Extended Data Fig.7a,b).
302
303 To identify molecular changes downstream of nicotine exposure, we performed cell type specific and
304 temporal DEG analyses (Extended datasheet 3). Since the nAChR subunits, CHRNA7 and
305 CHRFAM7A, were expressed by RG (Fig.2a-c), we investigated neurogenic dividing RG in cluster 9.
306 DEG analysis showed upregulation of genes involved in neurodevelopment, including NFIA, NFIB,

307 HNRNPU, FNBP1L, NBEA, AUST2, and PTPRZ1 (Fig.6d). NFIB is a transcription factor highly
308 expressed in progenitors[69]. HNRNPU, an RNA-binding protein, is associated with neurodevelopmental
309 disorders and seizures[70]. PTPRZ1 is a cell-surface protein enriched in oRG cells[71]. Genes
310 downregulated after nicotine treatment included CELSR3, H3C3, CIC, RAB11B, AGRN, B4GALNT1,
311 FLNA, L1CAM, NDRG4 and RUNDC3A (Fig. 6d). CELSR3 belongs to the cadherin receptor
312 superfamily and flamingo subfamily, implicated in neuronal migration and axon guidance[72,73]. CIC is a
313 transcriptional repressor regulating neural stem cell proliferation and neuronal differentiation[74,75].
314
315 To test nicotine exposure on early born excitatory neurons, we analyzed DEGs in cluster 0 post nicotine
316 exposure (Extended datasheet 3). Several genes, including NLGN4Y, ZEB2, CADM2, PBX1, PTBP2,
317 SNHG14, CTNND2, were upregulated (Fig.6e). PBX1 and PTBP2 act downstream of RNA-binding
318 protein PTBP1 and have been associated with neuronal differentiation[76]. SNHG14 is a long non-coding
319 RNA associated with the neurodevelopmental disorder Prader-Willi syndrome[77]. Several genes known
320 to be functionally critical and highly expressed in the cortex were also downregulated such as DCHS1,
321 SHANK3, LAMA5, NLGN2, LRP1, KIF1A (Fig.6e). DCHS1 is a cadherin protein involved in establishing
322 cortical architecture[78]. SHANK3 is involved in synapse formation and associated with ASD[79]. Similar
323 DEG analyses of gliogenic dividing RG identified chromatin regulators such as PRR12, EHMT2,
324 LENG8, and H1-10 to be upregulated post nicotine exposure (Extended datasheet 3). EHMT2 is a
325 potent regulator of gene transcription and methylates lysine 9 residues on histone H3 by recruiting
326 epigenetic regulators[80]. GO analysis underlined semaphorin-plexin axon guidance signaling to be highly
327 implicated downstream of nicotine exposure, in addition to processes such as cell adhesion, cell
328 motility, and extracellular-matrix (ECM) organization (Fig.6f). These findings emphasize that nicotine
329 exposure alters a variety of genes and processes critical for cortical development in a temporal and cell
330 type-specific manner.

331 We repeated our nicotine exposure experiments by exposing primary cortical cultures to low
332 concentrations of nicotine (10μM), approximating fetal exposure, for 5 days. We performed single-cell
333 sequencing using the Split-seq method (Extended data Fig. 8a) and collected approximately 20,000
334 cells from two biological replicates and their corresponding untreated controls. UMAP clustering
335 revealed distinct, well-known cell clusters (Extended data Fig. 8b), including RG, oRG, and various
336 neuronal subtypes. All cell clusters expressed established marker genes (Extended data Fig. 8c). DEG
337 analysis identified several key genes, such as effectors from the Semaphorin-Plexin pathway and the
338 Hippo ligand *DCHS1*. These changes in RG and Layer 5/6 excitatory neurons (EN) align with our
339 findings using higher concentrations (Fig. 6e,f, Extended Data Fig. 8d-g). Gene ontology analysis

340 highlighted Semaphorin-Plexin signaling, cell adhesion, and cytoskeletal organization in RG, while
341 Layer 5/6 excitatory neurons showed alterations in post-synaptic density, microtubule organization, and
342 synapse development (Extended Data Fig. 8e,g). Both high and low nicotine concentrations resulted in
343 consistent effects on RG and EN, including changes in the Hippo signaling effector, *DCHS1*.

344 ***Cell type specific differential gene expression following nAChR loss-of-function***

345 To investigate molecular changes upon loss-of-function of specific nAChR subunits, we identified cell-
346 type specific DEGs and associated GO processes after shRNA-mediated knockdown of CHRNA7 and
347 CHRFAM7A. Knockdown of CHRNA7 in neurogenic RG produced upregulation of EPHA6, ZEB2,
348 DAB1, and MYT1L, and downregulation of LAMA1, UBA7, and PLEKHM1 (Extended datasheet 3).
349 DAB1 protein plays a crucial role in reelin signaling during brain development[81]. MYT1L plays a key role
350 in neuronal differentiation by specifically repressing non-neuronal genes[82]. LAMA1 mediates cell
351 attachment, organization, and migration[83]. The associated GO processes for these DEGs include
352 lysosomal transport, neuron fate specification, axon guidance, and differentiation (Extended datasheet
353 3). The temporal shifts likely highlight differences in downstream molecular pathways between
354 neurogenic and gliogenic RG mediated by CHRNA7 and CHRFAM7A (Extended Data Fig. 9a-e).
355
356 Knockdown of CHRNA7 induced an upregulation of FAT3, RTN1, FBN2, SEL1L3, PCDH7 in oRGs
357 (Fig.6g), and associated processes included histone H3-K27 and lysine demethylation and negative
358 regulation of TGFβ signaling (Extended Data Fig.9b). Knockdown of CHRFAM7A in neurogenic oRG
359 led to an upregulation of genes including FAT3, ROBO2, CACNB2, KAZN, STOX1, PTPRM, FUT9,
360 FAT3, ADGRB3, CASC17, FBXL7, and downregulation of DNM3, GAP43, MAP7D1, DTX3L, NLRC5
361 (Fig.6h). FAT3, a Hippo signaling receptor, is a protocadherin involved in cortical development. Defects
362 in FAT3 genes are implicated in schizophrenia[84]. ADGRB3 is highly expressed in the brain and enriched
363 in the postsynaptic density (PSD), suggesting a role in synaptic signaling[85-87]. Other downregulated
364 genes relate to cytoskeletal organization, for example, GAP43 is highly expressed during brain
365 development and involved in neurite and synapse formation[88,89]. MAP7D1 is a microtubule associated
366 protein involved in microtubule stabilization and colossal axon elongation[90,91]. Other associated GO
367 processes include postsynaptic endocytosis, presynaptic vesicle budding, and dynamin family genes
368 involved in migration (Extended datasheet 3).
369
370 Knockdown of CHRFAM7A altered gene expression in GW19-22 Layer 5_6 ENs related to processes
371 such as pre- and post-synaptic membrane assembly, genetic imprinting, histone modification and
372 chromatin organization (Extended Data Fig.9c,d). In late, upper layer 2_3 ENs, processes affected by

373 CHRNA7 knockdown included generic neuron related functions such as synaptic membrane assembly,
374 endocytosis, and cell-cell adhesion (Extended Data Fig.9e). BMP and TGF signaling were also among
375 the processes affected post knockdown of CHRNA7, while loss of CHRFAM7A changed sterol transport
376 and PDGFRB pathways (Extended Data Fig.9e). Overall, we identified temporal and cell type specific
377 candidate genes and molecular processes post nAChR subunit manipulation, highlighting an ensemble
378 of candidate genes uniquely regulated by these receptors.
379
380 **Hippo signaling effector YAP1 is downstream of Cholinergic signaling**
381 Our DEG analyses identified several candidate genes that could be driving the downstream phenotypic
382 changes observed in our agonist and knockdown experiments. Notably, we found that nicotine
383 exposure downregulated the Hippo ligand DCHS1, while knockdown of both AChRs led to an
384 upregulation of the Hippo receptor FAT3 (Fig.6e, g-h). Yes-associated protein (YAP1), a co-activator in
385 the Hippo pathway, is a downstream effector known to regulate cell fate. Gain-of-function of Yap1
386 expands the stem cell pool and reduces neuronal populations[92-94], while Yap1 loss promotes neuronal
387 differentiation[94]. Nicotine exposure induces YAP1 expression and translocation to the nucleus[95]. To
388 explore this potential signaling crosstalk and impact on YAP1 protein, we treated cortical cultures from
389 GW16-19 (n=3 biological replicates) with agonists or shRNAs targeting CHRNA7, CHRFAM7A, or a
390 scrambled control. Protein lysates were collected on Day 5, and examined by Western blotting
391 (Fig.7a,b). We observed an increase in total YAP1 protein upon nicotine exposure and a reduction
392 following knockdown of CHRNA7 and CHRFAM7A (Fig.7b).
393
394 *In silico* analysis of published single-cell RNA-seq datasets revealed distinct expression patterns of
395 Hippo signaling components across cortical cell types[96] (Fig.7c). FAT3, CRB2 (Hippo receptors), and
396 YAP1 RNA were highly expressed in RG and oRG cells, whereas DCHS1 was ubiquitously expressed
397 across all cell types (Fig.7c). Immunostaining confirmed the expression of DCHS1 and YAP1 proteins in
398 the developing cortex (Fig.7d). DCHS1 was enriched in SOX2+ and EOMES+ cells in the VZ and inner
399 subventricular zone (ISVZ), with concentrated expression along apical endfeet, but was absent from the
400 oSVZ and CP. YAP1 expression also overlapped with SOX2+ and EOMES+ cells in the VZ/iSVZ/oSVZ,
401 but was undetectable in the CP. These findings support the progenitor-specific expression of YAP1
402 observed in our RNA-seq data (Fig.7d).
403
404 To further investigate the impact of cholinergic signaling on YAP1 and to explore potential rescue, we
405 treated organotypic cortical slices with the YAP1 inhibitor TAT-PDHPS1 in combination with ACh and
406 nicotine. TAT-PDHPS1 (TAT) is a peptide inhibitor that consists of a cell-penetrating peptide (TAT) and

407 an endogenous peptide (PDHPS1) known to inhibit YAP1 (Fig.7e). We compared the phenotypic
408 changes in treated samples with ACh, nicotine, and TAT treatment as well as untreated (UT) controls.
409 Both ACh and nicotine exposure resulted in upregulation of YAP1 expression, with increased nuclear
410 translocation of YAP1. TAT treatment induced cytoplasmic retention of YAP1, as expected. When
411 combined with ACh or nicotine, TAT reduced YAP1 expression and nuclear localization (Fig.7f).
412 Quantification of HOPX+ oRG cells in the oSVZ relative to total DAPI-stained cells revealed a
413 significant increase with both ACh and nicotine exposure. A complete rescue of oRG cell numbers was
414 observed in ACh+TAT-treated samples, while nicotine+TAT treatment resulted in partial rescue,
415 suggesting potential crosstalk between cholinergic and YAP1 signaling (Fig.7h). In contrast,
416 immunostaining for YAP1 revealed a significant loss of YAP1 protein in RFP+ cells following CHRNA7
417 and CHRFAM7A KD (Fig.7h). This corroborates our previous findings showing a reduction in YAP1
418 expression following AChR KD (Fig.7b).
419
420 Based on these observations, we propose a model of crosstalk between cholinergic signaling and the
421 Hippo effector YAP1. Upon cholinergic activation, YAP1 translocates to the nucleus, where it interacts
422 with transcription factors to regulate genes that balance stem cell maintenance and neurogenesis.
423 Activation by ACh and nicotine enhances YAP1 expression and promotes its nuclear translocation,
424 leading to an increase in RG at the expense of neurons. In contrast, nAChR knockdown reduces YAP1
425 expression and nuclear localization, shifting the balance toward neuronal differentiation and away from
426 RG maintenance (Fig. 8). Additionally, our loss-of-function experiments revealed a reduction in S100B+
427 astrocytes and OLIG2+ oligodendrocytes. These findings highlight the essential yet underexplored role
428 of cholinergic signaling in modulating Hippo pathway activity, influencing the fate of RG, oRG, and glial
429 cells, with potential implications for cortical development and disease.
430
431 **Discussion**
432 The cerebral cortex in humans is composed of billions of functionally distinct neurons that are formed in
433 a highly ordered manner during cortical development. Tightly regulated signaling cues are needed to
434 determine the diverse fates of progenitor cells and their progeny. In this study, we identify a new role of
435 nicotinic receptor signaling in regulating proliferation and neurogenesis of RG and oRG cells in
436 developing human cortex. We also use primary developing cortex and cortical organoids to
437 characterize the expression of the nAChR subunit, CHRNA7, which is broadly expressed in mammalian
438 brain, and CHRFAM7A, which is a human-specific gene arising from partial duplication of CHRNA7[24].
439 We used human *ex vivo* organotypic slices and organoids to model prenatal nicotine exposure. While
440 these systems offer valuable insights, they do have limitations. For example, the duration of drug

441 exposure was limited by the viability of our organotypic slices, and non-cortical brain regions that may
442 contribute to clinical phenotypes were not represented in our organoids.
443
444 CHRNA7 receptor subunits assemble to form pentameric α7 nAChRs. Previous studies have
445 demonstrated that the expression of α7 nAChR increases in the rodent brain until postnatal week 1,
446 after which it gradually decreases[13]. In the developing human cortex, nAChRs, including the α7
447 receptor, are present during the first trimester and increase in expression during later prenatal
448 development[97,98]. CHRFAM7A codes for the peptide subunit dupα7, that can assemble with the native
449 α7 subunit and negatively regulate receptor function in oocytes[27,28]. Despite previous research on the
450 function of CHRFAM7A, its expression and role in the developing cortex remains unclear. We found
451 robust expression of both nAChR subunits in SOX2+ RG progenitors in the VZ and oSVZ and observed
452 enrichment of CHRFAM7A in RG apical endfeet, hinting at potential signaling cues from the CSF.
453 Interestingly, choline, a selective α7 activator, is present in high concentrations in the developing human
454 brain[13,39,41] and we speculate it might be a source of cholinergic signaling in CSF. Another source of
455 cholinergic signaling could be the cholinergic fibers that course through the oSVZ at around GW15, the
456 IZ at around GW20, and the CP at later developmental stages. Overall, our results characterize the
457 expression of CHRNA7 and CHRFAM7A in the progenitor niches of the developing human cortex.
458
459 NAChRs regulate neural maturation and synaptic transmission[13,24], but their potential role in progenitor
460 cells during human cortical development is unclear. We show that activation of nAChRs with ACh and
461 nicotine results in a significant increase in the number of proliferating progenitor cells in primary
462 organotypic cortical slices and cortical organoids. The increase in progenitor cells is linked to a shift
463 from neurogenesis to increased progenitor cell self-renewal. The same effects were seen with
464 treatment of the α7 specific agonist PNU. Knockdown of the nAChR subunits CHRNA7 and
465 CHRFAM7A led to inverse phenotypes compared to activation of nAChRs, supporting a role for both
466 subunits in progenitor cell maintenance and neurogenesis.
467
468 Using bulk and single-nucleus RNA-sequencing, we obtained a more detailed understanding of the
469 genes and processes affected by specific nicotinic cholinergic receptor activation in RG and oRG cells.
470 The nAChR affected genes and GO processes involve cortical development and neurodevelopmental
471 disorders, highlighting the significance of cholinergic balance in the developing progenitor niches, with
472 potential clinical implications. Loss-of-function of CHRNA7 in neurogenic RG upregulated neuronal
473 migration and differentiation genes including FAT3, DAB1, MYTL1 and LAMA1[81-83,99,100]. Knockdown of
474 CHRFAM7A downregulated EGFR, CRB2, and FAT3, receptors involved in EGFR and Hippo signaling,

key pathways known to play roles in cell proliferation, migration, and differentiation[101,102] underscoring the role of CHRFAM7A in stem cell maintenance and neuronal differentiation. CHRFAM7A is formed from the partial duplication of CHRNA7 and appears to have acquired a differential role during human brain development. Our results suggest that cholinergic signaling cues are required to maintain balance between stem cell maintenance and neurogenesis during human cortical development.

A previous study found higher expression of CHRFAM7A and CHRFAM7A/CHRNA7 RNA ratios in prenatal compared to postnatal prefrontal cortex[30] and also found elevated levels of CHRFAM7A expression and reduced levels of CHRNA7 in postmortem brains of patients with schizophrenia[24,30]. Previous organoid studies have shown morphological abnormalities, including reduced size of neural progenitor-rich rosettes, altered proliferation, and reduction in neuron numbers in organoids derived from schizophrenia patients compared to healthy controls[103,104]. Based on our results showing a functional role of CHRFAM7A in proliferation and neurogenesis of cortical progenitors, we speculate that CHRFAM7A might play a role in the morphological abnormalities observed in patient organoids. Though CHRFAM7A is formed from the partial duplication of CHRNA7, it appears to have acquired a differential role during human cortical evolution. Since nAChRs are expressed on multiple cell types during development, and they have implications for disease pathology, it will be important to further study the role of specific nicotinic receptor subunits in other cell types in the developing human brain.

TKTL1 was among the genes downregulated by CHRFAM7A knockdown. Modern human TKTL1 differs from the archaic neanderthal gene by a single amino acid substitution[60]. Overexpression of the modern human TKTL1, but not the Neanderthal TKTL1, in developing mouse and ferret neocortex results in an increase in oRG cells and a presumed eventual increase in neuron number[60]. In our results, knockdown of the human-specific nAChR subunit, CHRFAM7A, caused downregulation of TKTL1, suggesting an evolutionarily important crosstalk. We identified twice as many exclusive DEGs following knockdown of CHRFAM7A (Extended datasheet 3). This strengthens our hypothesis that CHRFAM7A has acquired human-specific biological function.

The exposure of the developing fetus to nicotine through maternal smoking is known to lead to alterations in brain morphology, including reduced cortical grey matter volume and cortical thinning, as well as behavioral changes[6,7,9-12]. In this study we show that nicotine causes a shift from neurogenesis to progenitor self-renewal in primary human cortical tissue and organoids. Although the long-term consequences have not been explored, we speculate that a persistent shift away from neurogenesis, could underlie decreased cortical volume and cortical thinning in the offspring of smokers. Using

509 scRNAseq, we identified DEGs following nicotine exposure that could provide potential mechanisms for
510 the altered cortical development induced by maternal smoking. Our analyses identified Hippo signaling
511 effectors including FAT3, CRB2, DCHS1 and YAP1, to be downstream of nicotine-mediated cholinergic
512 activation. We observed an increase in YAP1 protein levels following nicotine exposure and a reduction
513 in YAP1 with AChR knockdown, along with corresponding changes in protein translocation. Mutations in
514 Hippo signaling effectors FAT2 and DCHS1 have been linked to Val-Maldergem syndrome, which is
515 characterized by periventricular heterotopias, cortical thinning, neuronal loss, and impaired neuronal
516 migration[92,94], partially overlapping with the reported effects of maternal smoking. Our findings reveal a
517 novel and previously unexplored signaling interaction between the cholinergic and Hippo pathways that
518 can influence the fate of RG and oRG cells, with potential pathological implications.
519
520 We identified several other genes affected by nicotine exposure that are linked to neurodevelopmental
521 diseases. For example, HNRNPU, upregulated by nicotine exposure, is involved in developmental and
522 epileptic encephalopathy[105] and AUTS2, also upregulated after nicotine exposure, is associated with
523 ASD and schizophrenia[106-108]. We also identified semaphorins and plexins to be affected after nicotine
524 exposure (Fig.6f, Extended Data Fig. 8e). Semaphorins and plexins are key regulators of cell
525 proliferation, axon guidance, neuronal migration, laminar segregation, central nervous system
526 patterning, and glial recruitment, all critical processes in cortical development[109]. We also observed an
527 upregulation of chromatin regulators in late stage dividing RG. GO analyses highlighted processes such
528 as chromatin silencing and organization, suggesting a vulnerability to chromatin-related dysregulation
529 post nicotine exposure (Extended datasheet 3). Our study aimed to identify selective transcriptional
530 changes and potential vulnerabilities of specific cell types to prenatal nicotine exposure. However, we
531 only investigated early and late second trimester cortical development. Future studies should address
532 effects at later stages of cortical development.
533
534 **Materials and Methods**
535 **Lead contact and materials availability**
536 Any questions and requests for resources should be directed to Arnold Kriegstein, at
537 Arnold.Kriegstein@ucsf.edu
538
539 *Pluripotent stem cell lines*
540 **Table 1.** Pluripotent stem cell lines

Cell line	Designation	Source	Identifiers	Additional

				Information
Cell line (*Homo sapiens)*	H1 / WA01 Embryonic stem cell line	WiCell	RRID:CVCL_9771	Male
Cell line (*Homo sapiens)*	WTC-11 induced pluripotent stem cell line	Conklin Laboratory (Gladstone Institutes)	GM25256	Male
Cell line (*Homo sapiens*)	1323-4 induced pluripotent stem cell line	Conklin lab (Gladstone Institute)	RRID:CVCL_0G84	Female

541

542 *Primary human cortex tissue*

543 Primary human cortical tissue was obtained and processed as approved by UCSF Gamete, Embryo
544 and Stem Cell Research Committee (GESCR). All samples were de-identified with no information on
545 sex. Tissue was collected with patient consent for research and in strict observance of legal,
546 institutional, and ethical regulations.

547

548 *Cortical organoid differentiation protocol*

549 Three PSCs (H1, 1323-4 and WTC11) were differentiated into cortical organoids based on a published
550 protocol for directed forebrain differentiation[42,110]. PSCs were dissociated into single cells using
551 accutase and plated into 96-well ultra-low attachment V-bottom plates at a density of about 10,000 cells
552 per well. Cells were aggregated in GMEM (Lifetech; #11710-035) containing 20% v/v Knockout Serum
553 Replacement (KSR; Lifetech; #10828-028), 1x Penicillin-Streptomycin (PS; Gibco), 1x non-essential
554 amino acids (Gibco), 11 mg/ml Sodium Pyruvate (Thermo Fisher; #11360070) and 0.1 mM 2-
555 Mercaptoethanol (Sigma). Fresh Rock inhibitor Y-27632 (20μM; Tocris; #1254), TGF-B inhibitor
556 SB431542 (5μM; Tocris; #1614) and WNT inhibitor IWR1-endo (3μM; Caymen Chem; #13659) were
557 added at every medium change until day 6, 18, and 18, respectively. Medium was changed every other
558 day. At day 18, cell aggregates were transferred to low adhesion 6-well plates and moved to an orbital
559 shaker rotating at 90 rpm. The culture medium was changed to DMEM/F-12 Glutamax (Gibco)
560 containing 1X N2 supplement (Lifetech, #17502-048), 1X CD Lipid concentrate (Lifetech; #11905-031),
561 1X PS and 2.5 μg/ml Amphotericin B (Gibco). At day 35, the medium was changed to DMEM/F-12
562 Glutamax containing 1X N2, 1X CD Lipid concentrate, 1x PS, 10% v/v Fetal bovine serum (FBS;
563 HyClone; #SH30071.03), 5μg/ml Heparin (Sigma; #H3149), 0.5% v/v growth-factor reduced Matrigel
564 and 2.5 μg/ml Amphotericin B. From day 70 onwards, cerebral organoids were maintained in DMEM/F-

565 12 Glutamax, 1X N2 supplement, 1X CD Lipid concentrate, 1X PS, 10% v/v FBS, 5 µg/ml Heparin, 1%
566 v/v growth-factor reduced Matrigel, 1X B27 supplement (Lifetech; #17504-044) and 2.5 µg/ml
567 Amphotericin B. All three PSC lines were utilized for treatment experiments in cortical organoids.
568
569 *Dissociation cultures*
570 Primary cortical tissue was cut into small pieces and dissociated using the Papain Dissociation system
571 (Worthington). Primary tissue was incubated in Papain (Worthington; #LK003178) resuspended in
572 Earle's Balanced Salt Solution (EBSS) and containing DNAse (Worthington; #LK003170) at 37°C for
573 30-40 mins. Falcon tubes were inverted 10 times every 10 mins. After incubation, samples were
574 mechanically triturated using a P1000 pipette to obtain a single cell suspension and spun down at 300g
575 for 5 mins. Supernatant was aspirated and cells were resuspended in DMEM/F-12 Glutamax containing
576 1X B27, 1X N2, 1X Sodium Pyruvate and 1X PS, filtered through 40µm nylon mesh cell strainers
577 (Fisherbrand) and counted. For qPCRs, 500,000 cells or 1 – 1.5 Mio. cells were plated for 12-well
578 plates or 6-well plates, respectively.
579
580 *Organotypic slice cultures*
581 Primary human cortical tissue was obtained in artificial cerebrospinal fluid (ACSF) containing 125 mm
582 NaCl, 2.5 mm KCl, 1 mm $MgCl_2$, 2 mm $CaCl_2$, 1.25 mm NaH_2PO_4, 25 mm $NaHCO_3$, 25 mm D-(+)-
583 glucose. ACSF was bubbled with a 95% O_2 - 5% CO_2 gas mixture before use. Tissue was embedded in
584 3.5% w/v low melt agarose (Fisher Scientific; BP165-25) and sectioned into 300 µm slices using a
585 vibratome (Leica). Slices were transferred to Millicell inserts in a 6-well plate and cultured at the air-
586 liquid interface with slice culture medium (66% v/v Basal Medium Eagle, 25% v/v Hank's Balanced Salt
587 solution, 5% v/v FBS, 0.67% w/v glucose, 1X Penicillin-Streptomycin-Glutamine, 1X N2 supplement).
588 Medium was changed every three days. For *ex vivo* knockdown assays, organotypic cortical slices
589 were infected with lentiviruses on day 0 and 4 and harvested for immunohistochemistry on day 7.
590
591 *Small molecule treatments*
592 Organotypic slices and iPSC-derived cerebral organoids were treated by daily addition of small
593 molecules to the respective culture medium for 4 days (as depicted in respective experimental
594 paradigms). Small molecules added were 10µM and 500µM (Tocris; #3546), 100µM acetylcholine
595 (ACh) (Tocris; #2809, 10µM PNU-282987 (PNU) (Tocris; #2303) or 5 µg/ml a-bungarotoxin () (Tocris;
596 #2133). PNU was dissolved in DMSO according to manufacturer's recommendation and all other small
597 molecules were dissolved in H_2O, thus, as a control, organotypic-slices and organoids were DMSO-

598 treated or untreated, respectively. YAP1 inhibitor, TAT-PDHPS1 (Tocris; #7832), 10umol/l was dissolved
599 in dissolved in H_2O, following the manufacturer's recommendation.
600
601 *RNAscope and BaseScope*
602 The RNAscope Multiplex Fluorescent Reagent Kit v2 and BaseScope Detection Reagent Kit v2 – RED
603 were purchased from ACD Advanced Cell Diagnostics. RNAscope was conducted for CHRNA7 and
604 BaseScope for CHRFAM7A according to the manufacturer's recommendation. BaseScope is used to
605 detect short target RNA sequences between 50-300 nucleotides. This technique is also used to detect
606 exon junctions and splice variants. Probes for CHRNA7 (Hs-CHRNA7; 310101, targeting 181-1591
607 region) and CHRFAM7A (BA-Hs-CHRFAM7A-E4E5; 704391, targeting 617-658 region) were
608 purchased from ACD biosciences. Opal 570 (Akoya Biosciences) was used as a fluorophore. After
609 RNAscope or BaseScope, immunohistochemistry was conducted as described below but without a
610 target retrieval step and using double the concentration of primary antibodies indicated in table 2**.**
611
612 *Immunohistochemistry*
613 Primary cortical tissue samples were fixed in 4% PFA overnight at 4°C, washed with 1x PBS and
614 equilibrated in 30% sucrose in 1x PBS overnight at 4°C. The samples were embedded in cryomolds in
615 3:2 O.C.T. (Tissue-tek) : 30% sucrose solution, cryopreserved on dry ice and stored at -80°C. Frozen
616 tissue was sectioned into 16µm sections onto Fisherbrand™ Superfrost™ glass slides and stored at -
617 80°C. Antigen-retrieval was performed with 1X boiling citric acid-based antigen unmasking solution
618 (Vector Laboratories) for 20 min. Slides were washed once with MilliQ-H_2O and twice with PBS and
619 blocked in Donkey blocking buffer (DBB) containing 5% donkey serum, 2% gelatin and 0.1% Triton X-
620 100 in PBS for 30 mins at RT. Primary antibodies (see table 2) were incubated in DBB overnight at 4°C,
621 washed three times with 0.1% Triton X-100 in PBS and incubated with AlexaFluor secondary antibodies
622 (ThermoFisher and Jackson Labs) in DBB for 3 hrs at RT. Organotypic slice cultures were processed
623 like primary cortical tissue, except that PFA fixation was conducted for 45 mins at room temperature
624 and slices were cryosectioned into 12µm sections. Cortical organoids were fixed, embedded,
625 sectioned, and stained like primary cortical tissue, except that they were fixed in 4% PFA for 45 mins at
626 room temperature, and processed into 14µm sections. Images were acquired using a Confocal
627 microscope (Leica TCS SP5 X).
628
629 **Table 2**. Antibodies used for immunohistochemistry.

Target Protein	Host species	Manufacturer	Identifier	Dilution

AChE	mouse	Abcam	ab2803	1:500
CHRFAM7A	rabbit	Aviva system biology	OAAN02465	1:250
CTIP2	rat	Abcam	ab18465	1:500
EOMES	sheep	R&D	AF6166	1:200
HOPX	rabbit	Proteintech	11419-1-AP	1:250
KI67	rat	Abcam	ab156956	1:300
NEUN	guinea pig	Millipore	ABN90	1:500
SOX2	mouse	Santa Cruz	Sc-365823	1:500
SATB2	mouse	Abcam	ab51502	1:500
VIMENTIN	chicken	EMD Millipore	Ab5733	1:250
ZO-1	rabbit	Proteintech	21773-1-AP	1:300
DLX5	rabbit	Sigma	HPA005670	1:100
YAP1	rabbit	Novus Biologicals	NB110-58358SS	1:300
DCHS1	rabbit	Novus Biologicals	NBP2-13901	1:300

TUNEL staining

Tissue slides were post-fixed with 4% PFA in TBS for 15-20mins at RT, washed in 1X TBS for 30mins and permeabilized using 0.1% Triton X-100 for 2mins. Slides were washed with TBS, each wash for 3mins, with 1X TBS. TUNEL mix from Roche In Situ Cell Death Detection Kit- FITC, composed of TUNEL label and enzyme were mixed in a proportion of 10:1, and added to slides for 1h at 37°C. Slides were washed 3X with TBS at RT for 5mins each, before mounting.

Western blotting

Protein lysates was prepared from primary tissue and organoids through trituration in RIPA buffer (Thermo Fisher; #89900) with complete protease inhibitor cocktail (Millipore-Sigma; #P8340-1ML). Samples were centrifuged at 12,000 g for 10 mins and the supernatant was used while the pellet was discarded. A protein mixture of 50:25:20:5 protein sample : NuPAGE LDS Sample Buffer (Invitrogen; #NP0008) : RIPA buffer : 2-mercaptoethanol was boiled at 95 – 98 °C for 10 mins and separated using 4-12% Polyacrylamide gels (Invitrogen; #NP0335BOX) in 1x NuPAGE MES SDS Running Buffer (Invitrogen; #NP0002) at 110V. Protein bands were transferred to Nitrocellulose membranes (Protan, GE) in MilliQ water containing 1x transfer buffer (Invitrogen; #NP00061) and 10% v/v methanol at 90V at 4°C for 1 hr. Membranes were blocked in blocking buffer (5% w/v milk powder in 1x tris buffered saline with Tween 20 (TBS-T) (Santa Cruz; #sc-362311 diluted in MilliQ-H_2O) for 1 hr at room

649 temperature and incubated at 4°C overnight in primary antibody diluted in blocking buffer (see table 3).
650 Membranes were washed three times for 15 min. in 1X TBS-T, incubated in secondary antibody (see
651 table 3) in blocking buffer for 2 hrs at room temperature and washed in 1X TBS-T three times for 15
652 min. Blots were detected using the SuperSignal™ West Pico PLUS Chemiluminescent Substrate
653 (Thermo Scientific; #34579) in a ChemiDoc MP UV-Vis Spectrometer (Bio-Rad).
654
655 **Table 3**. Western blotting antibodies

Primary / Secondary	**Target protein**	**Species**	**Manufacturer**	**Cat. #**	**dilution**
Primary	GAPDH	mouse	Sigma	G8975	1:5,000
Primary	HISTONE H3	mouse	Cell Signaling	3638S	1:1000
Primary	B-ACTIN	rabbit	Cell Signaling	4970S	1:1000
Primary	CHRNA7	rabbit	Alomone labs	ANC-007	1:500
Primary	CHRFAM7A	rabbit	Aviva system biology	OAAN02465	1:500
Primary	CHRNB1	rabbit	Proteintech	11553-1-AP	1:500
Primary	CHRNB2	rabbit	Abcam	ab41174	1:500
Secondary	Anti-Mouse HRP	rabbit	Abcam	ab6728	1:10,000
Secondary	Anti-Rabbit HRP	goat	Abcam	ab6721	1:10,000

656
657 *Pluripotent stem cell culture*
658 PSCs, frozen in mFreSR (Stem Cell Technologies; #5855), were thawed and cultured on growth-factor
659 reduced Matrigel (BD Biosciences; #354230)-coated six well plates in Stem Flex Pro Medium (Gibco)
660 with 10 μM Rock inhibitor Y-27632. Medium was changed every other day without Rock inhibitor until
661 the cells reached about 85-90% confluency. For maintenance passaging, ReLeSR (Stem Cell
662 Technologies; #100-0484) was added to cells for 1 min, aspirated, and cells were incubated at 37°C for
663 5 mins. Cells were resuspended in Stem Flex Pro Medium and plated into new growth-factor reduced
664 Matrigel-covered plates.
665
666 *Lentiviral Knockdown*
667 Multiple small hairpin-RNAs (shRNAs) directed against *CHRNA7* and *CHRFAM7A* were designed (see
668 table 4), and lentivirus generated and packaged in 293T cells. Supernatant was collected after 48 and

669 72h and ultracentrifuged. To test the knockdown efficiency using RT-qPCR, dissociated primary cortices
670 (GW14 -18) of three biological replicates was infected with lentiviruses carrying shRNAs, shCHRNA7
671 and shCHRFAM7A on day 0 and 3. shScrambled (shCONTROL) was used as a negative control for the
672 experiment. RNA was harvested for RT-qPCR on day 7.
673
674 **Table 4.** shRNA sequences

Target gene	Forward	ID
shCONTROL (pLKO-RFP)	CAACAAGATGAAGAGCACCAA	69040 (Addgene)
shCHRNA7_1	CCGGGCAAATGTCTTGGACAGATCACTCGAGTGATCTGTCCAAGACATTTGCTTTTTTG	TRCN0000434356 (Sigma ID)
shCHRNA7_2	CCGGGATCACTATTTACAGTGGAATCTCGAGATTCCACTGTAAATAGTGATCTTTTTG	TRCN0000061169 (Sigma ID)
shCHRNA7_3	CCGGCGAGTTCCAGAGGAAGCTTTACTCGAGTAAAGCTTCCTCTGGAACTCGTTTTTG	TRCN0000061170 (Sigma ID)
shCHRFAM7A_1	CCGGCAGAACCCATAGGACAAATAACTCGAGTTATTTGTCCTATGGGTTCTGTTTTTG	TRCN0000241872 (Sigma ID)
shCHRFAM7A_2	CCGGGGCAGATATCAGTGGCTATATCTCGAGATATAGCCACTGATATCTGCCTTTTTG	TRCN0000241869 (Sigma ID)
shCHRFAM7A_3	CCGGGCAAACTGCGATATTGCTGATCTCGAGATCAGCAATATCGCAGTTTGCTTTTTG	TRCN0000060468 (Sigma ID)

675
676 *RNA isolation and qPCR validation of candidate genes*
677 RNA was extracted from primary cortical tissue using the QIAGEN RNeasy Plus Micro Kit following the
678 manufacturer's recommendation. RNA concentrations were quantified using a NanoDrop. cDNA was
679 prepared using the SuperScript™ IV VILO™ Master Mix with ezDNase™ kit (Invitrogen; #11766050)
680 and qPCRs were performed with LightCycler® 480 SYBR Green I Master Kit (Roche; #4707516001).
681 Primers were designed and purchased from IDT and primer sequences for target genes are shown in
682 table 5.
683
684 **Table 5.** Primer sequences of target genes.

Target gene	Forward	Reverse
GAPDH	GGAGCGAGATCCCTCCAAAAT	GGCTGTTGTCATACTTCTCATGG

B-ACTIN	CATGTACGTTGCTATCCAGGC	CTCCTTAATGTCACGCACGAT
CHRNA7	GCTGGTCAAGAACTACAATCCC	CTCATCCACGTCCATGATCTG
CHRFAM7A	TGCATCTACCAGCATTTTCAGT	GCAATATCGCAGTTTGCAGCTAT
CACNA1A	TGGCACTCTACAACCCCATC	TCGGTGATCTTTTTGGCGTATT
BMP2	ACTACCAGAAACGAGTGGGAA	GCATCTGTTCTCGGAAAACCT
UNC5C	ACCTGTACTGTAAAGCAAGCC	GGACAATGAGACCGGAAGTTT
GABRG3	GTGGGTCTTGGCTCCAAAATC	ACGTCAATTACGGTCGGTTTTA
TKTL1	ACAAGCAGTCAGATCCAGAGA	TAGCTGGCCCTGTCGAAGTA
CXCL10	GTGGCATTCAAGGAGTACCTC	TGATGGCCTTCGATTCTGGATT
HTR2A	CTTTGTGCAGTCTGGATTTACCT	ACTGATATGGTCCAAACAGCAAT

Quantification Strategy

For small molecule experiments, immunohistochemistry was performed for known markers of radial glia, intermediate progenitors, proliferation, deep and upper layer neurons. Several sections across multiple biological replicates were imaged post immunohistochemistry. Quantifications were performed using IMARIS software and cell numbers were normalized by total number of DAPI per section. For knockdown experiments, the number of double positive cells in shCHRNA7 and shCHRFAM7A were normalized over total RFP positive (infected) cells and compared to shCONTROL. Each data point on every graph represents an image captured and quantified.

Bulk RNA sequencing

For bulk RNA samples, knockdown was performed in dissociated primary cultures using lentiviral-mediated shRNAs. Four biological (GW15, 18, 21, 22) and two technical replicates each were prepared, and RNA was isolated and purified as described for qPCR. For shRNAs and small molecule treatments, cells were harvested three- and four-days post treatments start, respectively. RNA samples were analyzed for their integrity and concentration using Agilent 2100 Bioanalyzer and only samples with RIN scores above 9.0 were processed for sequencing. Bulk RNA-sequencing was performed at Genewiz using 150bp paired-end RNA-seq on an Illumina Hi-Seq platform. Reads were aligned and quantified using kallisto and quantified at gene level with tximport. Differential gene expression analysis was performed using limma/voom, accounting for n=2 biological replicates per timepoint, with n=2 technical replicates within each individual. P values were corrected for multiple comparisons using the Benjamini-Hochberg false-discovery rate adjustment (Extended datasheet 2).

Single-cell sequencing

709 Primary cortical tissue corresponding to neurogenic-rich (GW15-18) and gliogenic-rich (GW19-23) time
710 points were dissociated and treated either with NIC or shRNAs on consecutive days as above. Cells
711 were harvested at day 5 and samples processed using the Parse Biosciences 100WTA kit according to
712 the manufacturer's recommendation. This method involves a combinatorial and sequential barcoding of
713 fixed cells or nuclei followed by generation of sublibraries. 8 sublibraries were prepared and tested with
714 BioAnalyzer for quality. Sequencing was performed using Illumina Nova-Seq S2 flow cell and data
715 analyzed using the Parse Computational pipelines.
716
717 *Bioinformatics Analysis- Bulk-RNAseq*
718 Reads were aligned and quantified using kallisto and quantified at gene level with tximport. Differential
719 gene expression analysis was performed using limma/voom, accounting for n=2 biological replicates
720 per timepoint, with n=2 technical replicates within each individual. P values were corrected for multiple
721 comparisons using the Benjamini-Hochberg false-discovery rate adjustment (Extended Datasheet 2).
722
723 *Bioinformatics Analysis - scRNAseq*
724 Nova-Seq data from 8 sublibraries were mapped to GRCh38/hg38 and demultiplexed using split-pipe[111]
725 (v1.1.1) from the parse biosciences pipeline with the following parameters: --mode all --chemistry v2 --
726 kit WT. Then the outputs of each sublibrary were combined into a single dataset using split-pipe --mode
727 comb. Gene expression matrices were loaded into the Python package Scanpy[112] (1.9.3) for quality
728 control and downstream analyses. We removed cells based on these criteria: (1) number of UMIs ≤
729 200, (2) number of UMIs ≥ 98-percentile, and (3) percentage of mitochondrial genes ≥ 20%. Cell
730 doublets were detected and removed using scvi-tools (0.20.3)[113]. Additionally, genes expressed in less
731 than 10 cells were discarded. Clean data were then normalized and transformed with Scanpy. Then we
732 leveraged scvi-tools to correct batch effects. To cluster the cells and identify cell types, we used Scanpy
733 for downstream analysis.
734 For differential genes analysis, FindMarkers from Seurat[114] (v4.3.0) was applied to compare two
735 conditions. We combined GW15 and GW16 as 2nd_early time point, and GW19 and GW22 as 2nd_late
736 time point. Genes with |log2FoldChange| > 0.25 and p.adjust <0.05 were considered as differentially
737 expressed genes. For GO terms enrichment, enrichR[115] (v3.2) and databases
738 "GO_Molecular_Function_2021", "GO_Cellular_Component_2021", "GO_Biological_Process_2021"
739 were used for functional enrichment.
740

741 *Quantifications and Statistics*

742 Quantifications were conducted manually using IMARIS Software. For statistical analysis, an unpaired
743 two-tailed student's t-test using prism software was used. For phenotypic analyses, to handle repeated
744 measures and paired samples when analyzing staining data, a linear mixed effect model [lme4 lmerTest
745 references] was used to statistically model the effect of agonist, antagonist, and shRNA knockdowns.
746 Staining was calculated as a percentage of DAPI cells within the image, which generated an
747 approximately normal distribution of values. Each staining was modeled as follows:

748 Percentage Positive ~ Condition + (1|Sample).

749 For a given protein stain, models were fit within each tissue type (Organoids week 4, Organoids Week
750 8, Slice cultures), with only relevant conditions. Untreated results was the background for results from
751 ACh, NIC, and BTX treatments, DMSO for PNU, and shCONTROL for shChRNA7 and shCHRFAM7A.

752 lme4: https://www.jstatsoft.org/article/view/v067i01[116]

753 lmerTest: https://www.jstatsoft.org/article/view/v082i13[117]

754 dharma: https://cran.r-project.org/web/packages/DHARMa/vignettes/DHARMa.html[118]

755 TUNEL staining was not normally distributed, because cell death was low, it generated more empty
756 values than expected by normal distribution. So instead, we took the mean for each sample/condition,
757 and conducted a paired, 2-tailed t test.

758

759 **Data Availability**

760 Original data from the study is available in Extended Datasheets 1, 2 and 3. RNA-seq data will be
761 available in dbGAP upon publication at dbGAP study accession: phs000989.v7.p1.

762

763 **References**

764 1 Heavner, W. E. & Smith, S. E. P. Resolving the Synaptic versus Developmental Dichotomy of
765 Autism Risk Genes. *Trends Neurosci* **43**, 227-241, doi:10.1016/j.tins.2020.01.009 (2020).
766 2 Kian, N., Samieefar, N. & Rezaei, N. Prenatal risk factors and genetic causes of ADHD in
767 children. *World J Pediatr* **18**, 308-319, doi:10.1007/s12519-022-00524-6 (2022).
768 3 Murray, R. M., Bhavsar, V., Tripoli, G. & Howes, O. 30 Years on: How the Neurodevelopmental
769 Hypothesis of Schizophrenia Morphed Into the Developmental Risk Factor Model of Psychosis.
770 *Schizophr Bull* **43**, 1190-1196, doi:10.1093/schbul/sbx121 (2017).
771 4 Lange, S., Probst, C., Rehm, J. & Popova, S. National, regional, and global prevalence of
772 smoking during pregnancy in the general population: a systematic review and meta-analysis.
773 *Lancet Glob Health* **6**, e769-e776, doi:10.1016/S2214-109X(18)30223-7 (2018).
774 5 Jafari, A. *et al.* National, regional, and global prevalence of cigarette smoking among
775 women/females in the general population: a systematic review and meta-analysis. *Environ*
776 *Health Prev Med* **26**, 5, doi:10.1186/s12199-020-00924-y (2021).
777 6 Holbrook, B. D. The effects of nicotine on human fetal development. *Birth Defects Res C*
778 *Embryo Today* **108**, 181-192, doi:10.1002/bdrc.21128 (2016).

7 Wickstrom, R. Effects of nicotine during pregnancy: human and experimental evidence. *Curr Neuropharmacol* **5**, 213-222, doi:10.2174/157015907781695955 (2007).
8 Brody, A. L. *et al.* Cigarette smoking saturates brain alpha 4 beta 2 nicotinic acetylcholine receptors. *Arch Gen Psychiatry* **63**, 907-915, doi:10.1001/archpsyc.63.8.907 (2006).
9 Anblagan, D. *et al.* Maternal smoking during pregnancy and fetal organ growth: a magnetic resonance imaging study. *PLoS One* **8**, e67223, doi:10.1371/journal.pone.0067223 (2013).
10 Roza, S. J. *et al.* Effects of maternal smoking in pregnancy on prenatal brain development. The Generation R Study. *Eur J Neurosci* **25**, 611-617, doi:10.1111/j.1460-9568.2007.05393.x (2007).
11 Zou, R. *et al.* Association of Maternal Tobacco Use During Pregnancy With Preadolescent Brain Morphology Among Offspring. *JAMA Netw Open* **5**, e2224701, doi:10.1001/jamanetworkopen.2022.24701 (2022).
12 El Marroun, H. *et al.* Prenatal tobacco exposure and brain morphology: a prospective study in young children. *Neuropsychopharmacology* **39**, 792-800, doi:10.1038/npp.2013.273 (2014).
13 Dwyer, J. B., Broide, R. S. & Leslie, F. M. Nicotine and brain development. *Birth Defects Res C Embryo Today* **84**, 30-44, doi:10.1002/bdrc.20118 (2008).
14 Trujillo, C. A. *et al.* Novel perspectives of neural stem cell differentiation: from neurotransmitters to therapeutics. *Cytometry A* **75**, 38-53, doi:10.1002/cyto.a.20666 (2009).
15 Slotkin, T. A. *et al.* Effects of prenatal nicotine exposure on primate brain development and attempted amelioration with supplemental choline or vitamin C: neurotransmitter receptors, cell signaling and cell development biomarkers in fetal brain regions of rhesus monkeys. *Neuropsychopharmacology* **30**, 129-144, doi:10.1038/sj.npp.1300544 (2005).
16 Nguyen, L. *et al.* Neurotransmitters as early signals for central nervous system development. *Cell Tissue Res* **305**, 187-202, doi:10.1007/s004410000343 (2001).
17 Atluri, P. *et al.* Functional nicotinic acetylcholine receptor expression in stem and progenitor cells of the early embryonic mouse cerebral cortex. *Dev Biol* **240**, 143-156, doi:10.1006/dbio.2001.0453 (2001).
18 Aramakis, V. B. & Metherate, R. Nicotine selectively enhances NMDA receptor-mediated synaptic transmission during postnatal development in sensory neocortex. *J Neurosci* **18**, 8485-8495 (1998).
19 Roerig, B. & Katz, L. C. Modulation of intrinsic circuits by serotonin 5-HT3 receptors in developing ferret visual cortex. *J Neurosci* **17**, 8324-8338 (1997).
20 Roerig, B., Nelson, D. A. & Katz, L. C. Fast synaptic signaling by nicotinic acetylcholine and serotonin 5-HT3 receptors in developing visual cortex. *J Neurosci* **17**, 8353-8362 (1997).
21 Slotkin, T. A. Cholinergic systems in brain development and disruption by neurotoxicants: nicotine, environmental tobacco smoke, organophosphates. *Toxicol Appl Pharmacol* **198**, 132-151, doi:10.1016/j.taap.2003.06.001 (2004).
22 Mudo, G., Belluardo, N., Mauro, A. & Fuxe, K. Acute intermittent nicotine treatment induces fibroblast growth factor-2 in the subventricular zone of the adult rat brain and enhances neuronal precursor cell proliferation. *Neuroscience* **145**, 470-483, doi:10.1016/j.neuroscience.2006.12.012 (2007).
23 Brooks, A. C. & Henderson, B. J. Systematic Review of Nicotine Exposure's Effects on Neural Stem and Progenitor Cells. *Brain Sci* **11**, doi:10.3390/brainsci11020172 (2021).
24 Sinkus, M. L. *et al.* The human CHRNA7 and CHRFAM7A genes: A review of the genetics, regulation, and function. *Neuropharmacology* **96**, 274-288, doi:10.1016/j.neuropharm.2015.02.006 (2015).
25 Caton, M., Ochoa, E. L. M. & Barrantes, F. J. The role of nicotinic cholinergic neurotransmission in delusional thinking. *NPJ Schizophr* **6**, 16, doi:10.1038/s41537-020-0105-9 (2020).
26 Zoli, M., Pucci, S., Vilella, A. & Gotti, C. Neuronal and Extraneuronal Nicotinic Acetylcholine Receptors. *Curr Neuropharmacol* **16**, 338-349, doi:10.2174/1570159X15666170912110450 (2018).

27 Araud, T. *et al.* The chimeric gene CHRFAM7A, a partial duplication of the CHRNA7 gene, is a dominant negative regulator of alpha7*nAChR function. *Biochem Pharmacol* **82**, 904-914, doi:10.1016/j.bcp.2011.06.018 (2011).
28 Wang, Y. *et al.* The duplicated alpha7 subunits assemble and form functional nicotinic receptors with the full-length alpha7. *J Biol Chem* **289**, 26451-26463, doi:10.1074/jbc.M114.582858 (2014).
29 Di Lascio, S., Fornasari, D. & Benfante, R. The Human-Restricted Isoform of the alpha7 nAChR, CHRFAM7A: A Double-Edged Sword in Neurological and Inflammatory Disorders. *Int J Mol Sci* **23**, doi:10.3390/ijms23073463 (2022).
30 Kunii, Y. *et al.* CHRNA7 and CHRFAM7A mRNAs: co-localized and their expression levels altered in the postmortem dorsolateral prefrontal cortex in major psychiatric disorders. *Am J Psychiatry* **172**, 1122-1130, doi:10.1176/appi.ajp.2015.14080978 (2015).
31 Lee, C. H. & Hung, S. Y. Physiologic Functions and Therapeutic Applications of alpha7 Nicotinic Acetylcholine Receptor in Brain Disorders. *Pharmaceutics* **15**, doi:10.3390/pharmaceutics15010031 (2022).
32 Hogg, R. C., Raggenbass, M. & Bertrand, D. Nicotinic acetylcholine receptors: from structure to brain function. *Rev Physiol Biochem Pharmacol* **147**, 1-46, doi:10.1007/s10254-003-0005-1 (2003).
33 Koulousakis, P., Andrade, P., Visser-Vandewalle, V. & Sesia, T. The Nucleus Basalis of Meynert and Its Role in Deep Brain Stimulation for Cognitive Disorders: A Historical Perspective. *J Alzheimers Dis* **69**, 905-919, doi:10.3233/JAD-180133 (2019).
34 Candy, J. M. *et al.* Evidence for the early prenatal development of cortical cholinergic afferents from the nucleus of Meynert in the human foetus. *Neurosci Lett* **61**, 91-95, doi:10.1016/0304-3940(85)90406-9 (1985).
35 Mesulam, M. M. The cholinergic innervation of the human cerebral cortex. *Prog Brain Res* **145**, 67-78, doi:10.1016/S0079-6123(03)45004-8 (2004).
36 Lui, J. H., Hansen, D. V. & Kriegstein, A. R. Development and evolution of the human neocortex. *Cell* **146**, 18-36, doi:10.1016/j.cell.2011.06.030 (2011).
37 Hansen, D. V., Lui, J. H., Parker, P. R. & Kriegstein, A. R. Neurogenic radial glia in the outer subventricular zone of human neocortex. *Nature* **464**, 554-561, doi:10.1038/nature08845 (2010).
38 Ellis, P. *et al.* SOX2, a persistent marker for multipotential neural stem cells derived from embryonic stem cells, the embryo or the adult. *Dev Neurosci* **26**, 148-165, doi:10.1159/000082134 (2004).
39 Albuquerque, E. X., Pereira, E. F., Braga, M. F. & Alkondon, M. Contribution of nicotinic receptors to the function of synapses in the central nervous system: the action of choline as a selective agonist of alpha 7 receptors. *J Physiol Paris* **92**, 309-316, doi:10.1016/s0928-4257(98)80039-9 (1998).
40 Girard, N. *et al.* Assessment of normal fetal brain maturation in utero by proton magnetic resonance spectroscopy. *Magn Reson Med* **56**, 768-775, doi:10.1002/mrm.21017 (2006).
41 Zeisel, S. H. Choline: critical role during fetal development and dietary requirements in adults. *Annu Rev Nutr* **26**, 229-250, doi:10.1146/annurev.nutr.26.061505.111156 (2006).
42 Kadoshima, T. *et al.* Self-organization of axial polarity, inside-out layer pattern, and species-specific progenitor dynamics in human ES cell-derived neocortex. *Proc Natl Acad Sci U S A* **110**, 20284-20289, doi:10.1073/pnas.1315710110 (2013).
43 Lancaster, M. A. *et al.* Cerebral organoids model human brain development and microcephaly. *Nature* **501**, 373-379, doi:10.1038/nature12517 (2013).
44 Bhaduri, A. *et al.* Cell stress in cortical organoids impairs molecular subtype specification. *Nature* **578**, 142-148, doi:10.1038/s41586-020-1962-0 (2020).
45 Tiwari, R. K., Sharma, V., Pandey, R. K. & Shukla, S. S. Nicotine Addiction: Neurobiology and Mechanism. *J Pharmacopuncture* **23**, 1-7, doi:10.3831/KPI.2020.23.001 (2020).

46 Aryal, S. P. *et al.* Nicotine induces morphological and functional changes in astrocytes via nicotinic receptor activity. *Glia* **69**, 2037-2053, doi:10.1002/glia.24011 (2021).
47 Huang, B. *et al.* Demyelination in the medial prefrontal cortex by withdrawal from chronic nicotine causes impaired cognitive memory. *Prog Neuropsychopharmacol Biol Psychiatry* **129**, 110901, doi:10.1016/j.pnpbp.2023.110901 (2024).
48 Young, H. S., Herbette, L. G. & Skita, V. Alpha-bungarotoxin binding to acetylcholine receptor membranes studied by low angle X-ray diffraction. *Biophys J* **85**, 943-953, doi:10.1016/S0006-3495(03)74533-0 (2003).
49 Indelicato, E. & Boesch, S. From Genotype to Phenotype: Expanding the Clinical Spectrum of CACNA1A Variants in the Era of Next Generation Sequencing. *Front Neurol* **12**, 639994, doi:10.3389/fneur.2021.639994 (2021).
50 Wetzel-Smith, M. K. *et al.* A rare mutation in UNC5C predisposes to late-onset Alzheimer's disease and increases neuronal cell death. *Nat Med* **20**, 1452-1457, doi:10.1038/nm.3736 (2014).
51 Kim, D. & Ackerman, S. L. The UNC5C netrin receptor regulates dorsal guidance of mouse hindbrain axons. *J Neurosci* **31**, 2167-2179, doi:10.1523/JNEUROSCI.5254-10.2011 (2011).
52 Coskunpinar, E. M., Tur, S., Cevher Binici, N. & Yazan Songur, C. Association of GABRG3, GABRB3, HTR2A gene variants with autism spectrum disorder. *Gene* **870**, 147399, doi:10.1016/j.gene.2023.147399 (2023).
53 Lohmann, K. *et al.* Novel GNB1 mutations disrupt assembly and function of G protein heterotrimers and cause global developmental delay in humans. *Hum Mol Genet* **26**, 1078-1086, doi:10.1093/hmg/ddx018 (2017).
54 Ozeki, Y. *et al.* A novel balanced chromosomal translocation found in subjects with schizophrenia and schizotypal personality disorder: altered l-serine level associated with disruption of PSAT1 gene expression. *Neurosci Res* **69**, 154-160, doi:10.1016/j.neures.2010.10.003 (2011).
55 Andrews, M. G. *et al.* LIF signaling regulates outer radial glial to interneuron fate during human cortical development. *Cell Stem Cell* **30**, 1382-1391 e1385, doi:10.1016/j.stem.2023.08.009 (2023).
56 Wang, W. A., Groenendyk, J. & Michalak, M. Calreticulin signaling in health and disease. *Int J Biochem Cell Biol* **44**, 842-846, doi:10.1016/j.biocel.2012.02.009 (2012).
57 Reid, K. M., Kitchener, E. J. A., Butler, C. A., Cockram, T. O. J. & Brown, G. C. Brain Cells Release Calreticulin That Attracts and Activates Microglia, and Inhibits Amyloid Beta Aggregation and Neurotoxicity. *Front Immunol* **13**, 859686, doi:10.3389/fimmu.2022.859686 (2022).
58 Kirkpatrick, L. L., Matzuk, M. M., Dodds, D. C. & Perin, M. S. Biochemical interactions of the neuronal pentraxins. Neuronal pentraxin (NP) receptor binds to taipoxin and taipoxin-associated calcium-binding protein 49 via NP1 and NP2. *J Biol Chem* **275**, 17786-17792, doi:10.1074/jbc.M002254200 (2000).
59 Ebendal, T., Bengtsson, H. & Soderstrom, S. Bone morphogenetic proteins and their receptors: potential functions in the brain. *J Neurosci Res* **51**, 139-146, doi:10.1002/(SICI)1097-4547(19980115)51:2<139::AID-JNR2>3.0.CO;2-E (1998).
60 Pinson, A. *et al.* Human TKTL1 implies greater neurogenesis in frontal neocortex of modern humans than Neanderthals. *Science* **377**, eabl6422, doi:10.1126/science.abl6422 (2022).
61 Lee, S. *et al.* Lipocalin-2 Is a chemokine inducer in the central nervous system: role of chemokine ligand 10 (CXCL10) in lipocalin-2-induced cell migration. *J Biol Chem* **286**, 43855-43870, doi:10.1074/jbc.M111.299248 (2011).
62 Hirth, M. *et al.* CXCL10 and CCL21 Promote Migration of Pancreatic Cancer Cells Toward Sensory Neurons and Neural Remodeling in Tumors in Mice, Associated With Pain in Patients. *Gastroenterology* **159**, 665-681 e613, doi:10.1053/j.gastro.2020.04.037 (2020).

63 Klein, R. S. *et al.* Neuronal CXCL10 directs CD8+ T-cell recruitment and control of West Nile virus encephalitis. *J Virol* **79**, 11457-11466, doi:10.1128/JVI.79.17.11457-11466.2005 (2005).
64 Mirones, I. *et al.* A role for the CXCR3/CXCL10 axis in Rasmussen encephalitis. *Pediatr Neurol* **49**, 451-457 e451, doi:10.1016/j.pediatrneurol.2013.07.019 (2013).
65 Mayer, S. *et al.* Multimodal Single-Cell Analysis Reveals Physiological Maturation in the Developing Human Neocortex. *Neuron* **102**, 143-158 e147, doi:10.1016/j.neuron.2019.01.027 (2019).
66 Mattina, G. F., Samaan, Z., Hall, G. B. & Steiner, M. The association of HTR2A polymorphisms with obsessive-compulsive disorder and its subtypes: A meta-analysis. *J Affect Disord* **275**, 278-289, doi:10.1016/j.jad.2020.06.016 (2020).
67 Fabbri, C., Marsano, A. & Serretti, A. Genetics of serotonin receptors and depression: state of the art. *Curr Drug Targets* **14**, 531-548, doi:10.2174/1389450111314050004 (2013).
68 Andrews, M. G. *et al.* Tropism of SARS-CoV-2 for human cortical astrocytes. *Proc Natl Acad Sci U S A* **119**, e2122236119, doi:10.1073/pnas.2122236119 (2022).
69 Bunt, J. *et al.* Combined allelic dosage of Nfia and Nfib regulates cortical development. *Brain Neurosci Adv* **1**, 2398212817739433, doi:10.1177/2398212817739433 (2017).
70 Gillentine, M. A. *et al.* Rare deleterious mutations of HNRNP genes result in shared neurodevelopmental disorders. *Genome Med* **13**, 63, doi:10.1186/s13073-021-00870-6 (2021).
71 Pollen, A. A. *et al.* Molecular identity of human outer radial glia during cortical development. *Cell* **163**, 55-67, doi:10.1016/j.cell.2015.09.004 (2015).
72 Chai, G., Goffinet, A. M. & Tissir, F. Celsr3 and Fzd3 in axon guidance. *Int J Biochem Cell Biol* **64**, 11-14, doi:10.1016/j.biocel.2015.03.013 (2015).
73 Hakanen, J. *et al.* The Celsr3-Kif2a axis directs neuronal migration in the postnatal brain. *Prog Neurobiol* **208**, 102177, doi:10.1016/j.pneurobio.2021.102177 (2022).
74 Hwang, I. *et al.* CIC is a critical regulator of neuronal differentiation. *JCI Insight* **5**, doi:10.1172/jci.insight.135826 (2020).
75 Ahmad, S. T. *et al.* Capicua regulates neural stem cell proliferation and lineage specification through control of Ets factors. *Nat Commun* **10**, 2000, doi:10.1038/s41467-019-09949-6 (2019).
76 Linares, A. J. *et al.* The splicing regulator PTBP1 controls the activity of the transcription factor Pbx1 during neuronal differentiation. *Elife* **4**, e09268, doi:10.7554/eLife.09268 (2015).
77 Ariyanfar, S. & Good, D. J. Analysis of SNHG14: A Long Non-Coding RNA Hosting SNORD116, Whose Loss Contributes to Prader-Willi Syndrome Etiology. *Genes (Basel)* **14**, doi:10.3390/genes14010097 (2022).
78 Beste, C., Ocklenburg, S., von der Hagen, M. & Di Donato, N. Mammalian cadherins DCHS1-FAT4 affect functional cerebral architecture. *Brain Struct Funct* **221**, 2487-2491, doi:10.1007/s00429-015-1051-6 (2016).
79 Peca, J. *et al.* Shank3 mutant mice display autistic-like behaviours and striatal dysfunction. *Nature* **472**, 437-442, doi:10.1038/nature09965 (2011).
80 Deimling, S. J., Olsen, J. B. & Tropepe, V. The expanding role of the Ehmt2/G9a complex in neurodevelopment. *Neurogenesis (Austin)* **4**, e1316888, doi:10.1080/23262133.2017.1316888 (2017).
81 Feng, L. & Cooper, J. A. Dual functions of Dab1 during brain development. *Mol Cell Biol* **29**, 324-332, doi:10.1128/MCB.00663-08 (2009).
82 Mall, M. *et al.* Myt1l safeguards neuronal identity by actively repressing many non-neuronal fates. *Nature* **544**, 245-249, doi:10.1038/nature21722 (2017).
83 Aumailley, M. The laminin family. *Cell Adh Migr* **7**, 48-55, doi:10.4161/cam.22826 (2013).
84 Yan, P. *et al.* An Association Study Between Genetic Polymorphisms in Functional Regions of Five Genes and the Risk of Schizophrenia. *J Mol Neurosci* **59**, 366-375, doi:10.1007/s12031-016-0751-6 (2016).

85 Collins, M. O. *et al.* Molecular characterization and comparison of the components and multiprotein complexes in the postsynaptic proteome. *J Neurochem* **97 Suppl 1**, 16-23, doi:10.1111/j.1471-4159.2005.03507.x (2006).
86 Stephenson, J. R. *et al.* Brain-specific angiogenesis inhibitor-1 signaling, regulation, and enrichment in the postsynaptic density. *J Biol Chem* **288**, 22248-22256, doi:10.1074/jbc.M113.489757 (2013).
87 Duman, J. G., Tu, Y. K. & Tolias, K. F. Emerging Roles of BAI Adhesion-GPCRs in Synapse Development and Plasticity. *Neural Plast* **2016**, 8301737, doi:10.1155/2016/8301737 (2016).
88 Benowitz, L. I. & Perrone-Bizzozero, N. I. The expression of GAP-43 in relation to neuronal growth and plasticity: when, where, how, and why? *Prog Brain Res* **89**, 69-87, doi:10.1016/s0079-6123(08)61716-1 (1991).
89 Rosskothen-Kuhl, N. & Illing, R. B. Gap43 transcription modulation in the adult brain depends on sensory activity and synaptic cooperation. *PLoS One* **9**, e92624, doi:10.1371/journal.pone.0092624 (2014).
90 Kikuchi, K. *et al.* Map7D2 and Map7D1 facilitate microtubule stabilization through distinct mechanisms in neuronal cells. *Life Sci Alliance* **5**, doi:10.26508/lsa.202201390 (2022).
91 Koizumi, H. *et al.* DCLK1 phosphorylates the microtubule-associated protein MAP7D1 to promote axon elongation in cortical neurons. *Dev Neurobiol* **77**, 493-510, doi:10.1002/dneu.22428 (2017).
92 Cappello, S. *et al.* Mutations in genes encoding the cadherin receptor-ligand pair DCHS1 and FAT4 disrupt cerebral cortical development. *Nat Genet* **45**, 1300-1308, doi:10.1038/ng.2765 (2013).
93 Kostic, M. *et al.* YAP Activity Is Necessary and Sufficient for Basal Progenitor Abundance and Proliferation in the Developing Neocortex. *Cell Rep* **27**, 1103-1118 e1106, doi:10.1016/j.celrep.2019.03.091 (2019).
94 Mukhtar, T. *et al.* Tead transcription factors differentially regulate cortical development. *Sci Rep* **10**, 4625, doi:10.1038/s41598-020-61490-5 (2020).
95 Ben, Q. *et al.* A nicotine-induced positive feedback loop between HIF1A and YAP1 contributes to epithelial-to-mesenchymal transition in pancreatic ductal adenocarcinoma. *J Exp Clin Cancer Res* **39**, 181, doi:10.1186/s13046-020-01689-6 (2020).
96 Wang, L. *et al.* Molecular and cellular dynamics of the developing human neocortex at single-cell resolution. *bioRxiv*, doi:10.1101/2024.01.16.575956 (2024).
97 Falk, L., Nordberg, A., Seiger, A., Kjaeldgaard, A. & Hellstrom-Lindahl, E. The alpha7 nicotinic receptors in human fetal brain and spinal cord. *J Neurochem* **80**, 457-465, doi:10.1046/j.0022-3042.2001.00714.x (2002).
98 Hellstrom-Lindahl, E., Gorbounova, O., Seiger, A., Mousavi, M. & Nordberg, A. Regional distribution of nicotinic receptors during prenatal development of human brain and spinal cord. *Brain Res Dev Brain Res* **108**, 147-160, doi:10.1016/s0165-3806(98)00046-7 (1998).
99 Micalizzi, A. *et al.* Clinical, neuroradiological and molecular characterization of cerebellar dysplasia with cysts (Poretti-Boltshauser syndrome). *Eur J Hum Genet* **24**, 1262-1267, doi:10.1038/ejhg.2016.19 (2016).
100 Kamate, M., Goudar, N. & Hattiholi, V. Antenatal presentation and supratentorial brain abnormalities in a child with Poretti-Boltshauser syndrome. *Brain Dev* **44**, 139-141, doi:10.1016/j.braindev.2021.09.010 (2022).
101 Ouyang, T., Meng, W., Li, M., Hong, T. & Zhang, N. Recent Advances of the Hippo/YAP Signaling Pathway in Brain Development and Glioma. *Cell Mol Neurobiol* **40**, 495-510, doi:10.1007/s10571-019-00762-9 (2020).
102 Romano, R. & Bucci, C. Role of EGFR in the Nervous System. *Cells* **9**, doi:10.3390/cells9081887 (2020).

103 Notaras, M. *et al.* Schizophrenia is defined by cell-specific neuropathology and multiple neurodevelopmental mechanisms in patient-derived cerebral organoids. *Mol Psychiatry* **27**, 1416-1434, doi:10.1038/s41380-021-01316-6 (2022).
104 Stachowiak, E. K. *et al.* Cerebral organoids reveal early cortical maldevelopment in schizophrenia-computational anatomy and genomics, role of FGFR1. *Transl Psychiatry* **7**, 6, doi:10.1038/s41398-017-0054-x (2017).
105 Sapir, T. *et al.* Heterogeneous nuclear ribonucleoprotein U (HNRNPU) safeguards the developing mouse cortex. *Nat Commun* **13**, 4209, doi:10.1038/s41467-022-31752-z (2022).
106 Hori, K., Shimaoka, K. & Hoshino, M. AUTS2 Gene: Keys to Understanding the Pathogenesis of Neurodevelopmental Disorders. *Cells* **11**, doi:10.3390/cells11010011 (2021).
107 Sultana, R. *et al.* Identification of a novel gene on chromosome 7q11.2 interrupted by a translocation breakpoint in a pair of autistic twins. *Genomics* **80**, 129-134, doi:10.1006/geno.2002.6810 (2002).
108 Zhang, B. *et al.* Association study identifying a new susceptibility gene (AUTS2) for schizophrenia. *Int J Mol Sci* **15**, 19406-19416, doi:10.3390/ijms151119406 (2014).
109 Limoni, G. & Niquille, M. Semaphorins and Plexins in central nervous system patterning: the key to it all? *Curr Opin Neurobiol* **66**, 224-232, doi:10.1016/j.conb.2020.12.014 (2021).
110 Pollen, A. A. *et al.* Establishing Cerebral Organoids as Models of Human-Specific Brain Evolution. *Cell* **176**, 743-756 e717, doi:10.1016/j.cell.2019.01.017 (2019).
111 Tran, V. *et al.* High sensitivity single cell RNA sequencing with split pool barcoding. *bioRxiv*, doi:https://doi.org/10.1101/2022.08.27.505512 (2022).
112 Wolf, F. A., Angerer, P. & Theis, F. J. SCANPY: large-scale single-cell gene expression data analysis. *Genome Biol* **19**, 15, doi:10.1186/s13059-017-1382-0 (2018).
113 Gayoso, A. *et al.* A Python library for probabilistic analysis of single-cell omics data. *Nat Biotechnol* **40**, 163-166, doi:10.1038/s41587-021-01206-w (2022).
114 Hao, Y. *et al.* Integrated analysis of multimodal single-cell data. *Cell* **184**, 3573-3587 e3529, doi:10.1016/j.cell.2021.04.048 (2021).
115 Xie, Z. *et al.* Gene Set Knowledge Discovery with Enrichr. *Curr Protoc* **1**, e90, doi:10.1002/cpz1.90 (2021).
116 https://www.jstatsoft.org/article/view/v067i01.
117 https://www.jstatsoft.org/article/view/v082i13.
118 https://cran.r-project.org/web/packages/DHARMa/vignettes/DHARMa.html.

ACKNOWLEDGEMENTS

The authors thank Dr. Arpana Arjun and members of the A.R.K laboratory for useful discussions. This study was supported by the NIH award R35NS097305 to A.R.K. and by Boehringer Ingelheim Fonds PhD Fellowship to C.V.S.

AUTHOR CONTRIBUTIONS

Author contributions: T.M., M.P.P., C.V.S., M.K.H, J.L., and A.R.K. designed research; T.M., C.V.S., M.W., J.R., S.W., Q.B., J.B., V.U., M.S., L.Z., I.L.C., I.M., M.A.A and L.Z. performed research; Y.W., T.M., C.V.S., M.P.P., G.Z., V.U., M.S., M.W., and J.B., analyzed data; C.V.S., T.M., Y.W., M.P.P., and A.R.K. wrote the paper; and T.M. and A.R.K. supervised.

CONFLICTING INTERESTS

A.R.K is a co-founder, consultant, and member of the Board for Neurona Therapeutics. The other authors declare no conflicting interests.

Fig. 1: Acetylcholinesterase co-localizes with HOPX+ outer radial glia in the oSVZ

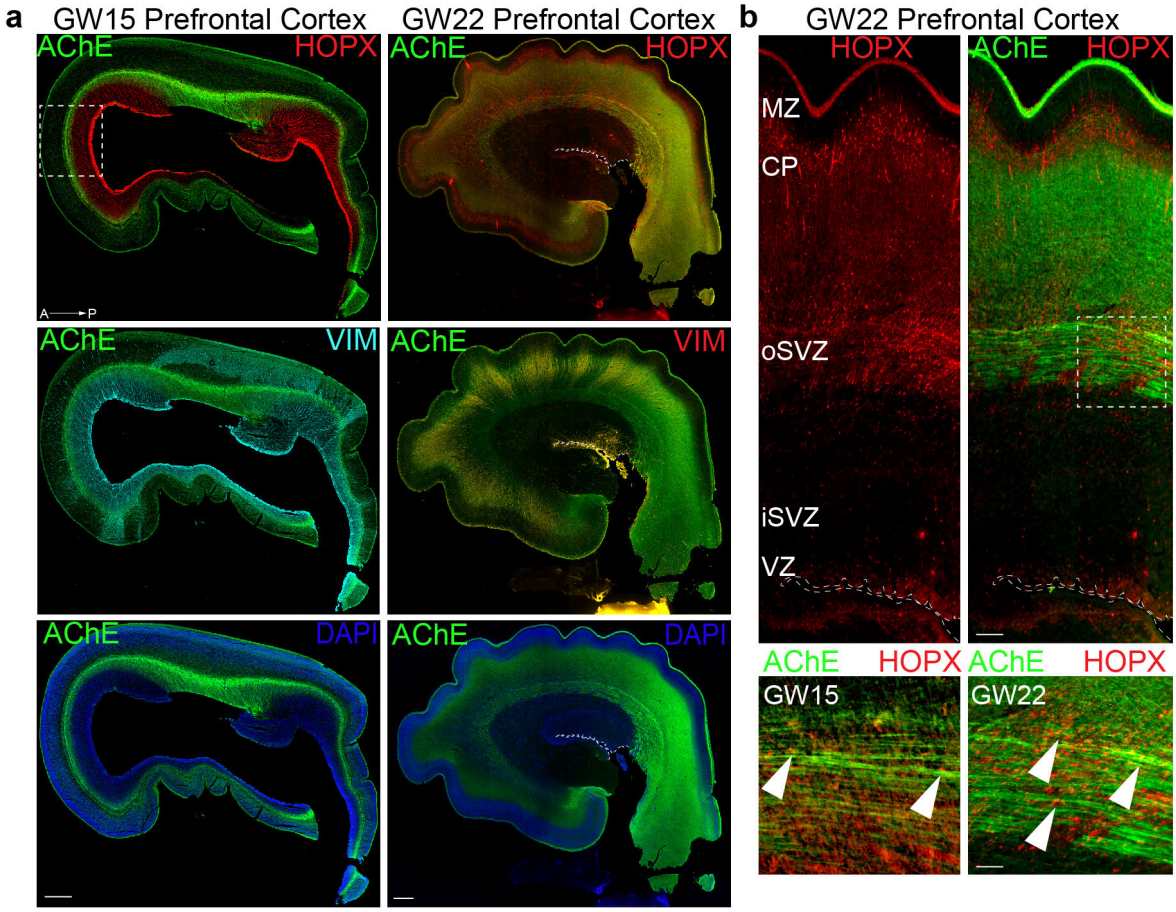

Fig. 1. Acetylcholinesterase (AChE) is expressed in the developing prefrontal cortex throughout cortical development (GW15-22). a. Representative images showing immunostaining of AChE+ cholinergic fibers, HOPX+ outer radial glia and vimentin (VIM)+ radial glia fibers at GW15, and GW22. Scale bar = 500um. **b.** AChE co-localizes with HOPX+ outer radial glia in the oSVZ. Representative images of GW15 and GW22 prefrontal cortex at higher magnification show overlap of HOPX+ oRG and AChE+ cholinergic fibers. Arrowheads show co-expression of HOPX and AChE. Scale bar = 200um and 100um. Abbreviations : A-P (anterior-posterior), ventricular zone (VZ), inner subventricular zone (iSVZ), outer subventricular zone (oSVZ) and Cortical plate (CP).

Fig.2. Cholinergic Receptor subunits CHRNA7 and CHRFAM7A are expressed in progenitor niches

a CHRNA7 and CHRFAM7A RNA expression

c Human-specific CHRFAM7A protein is enriched in the VZ

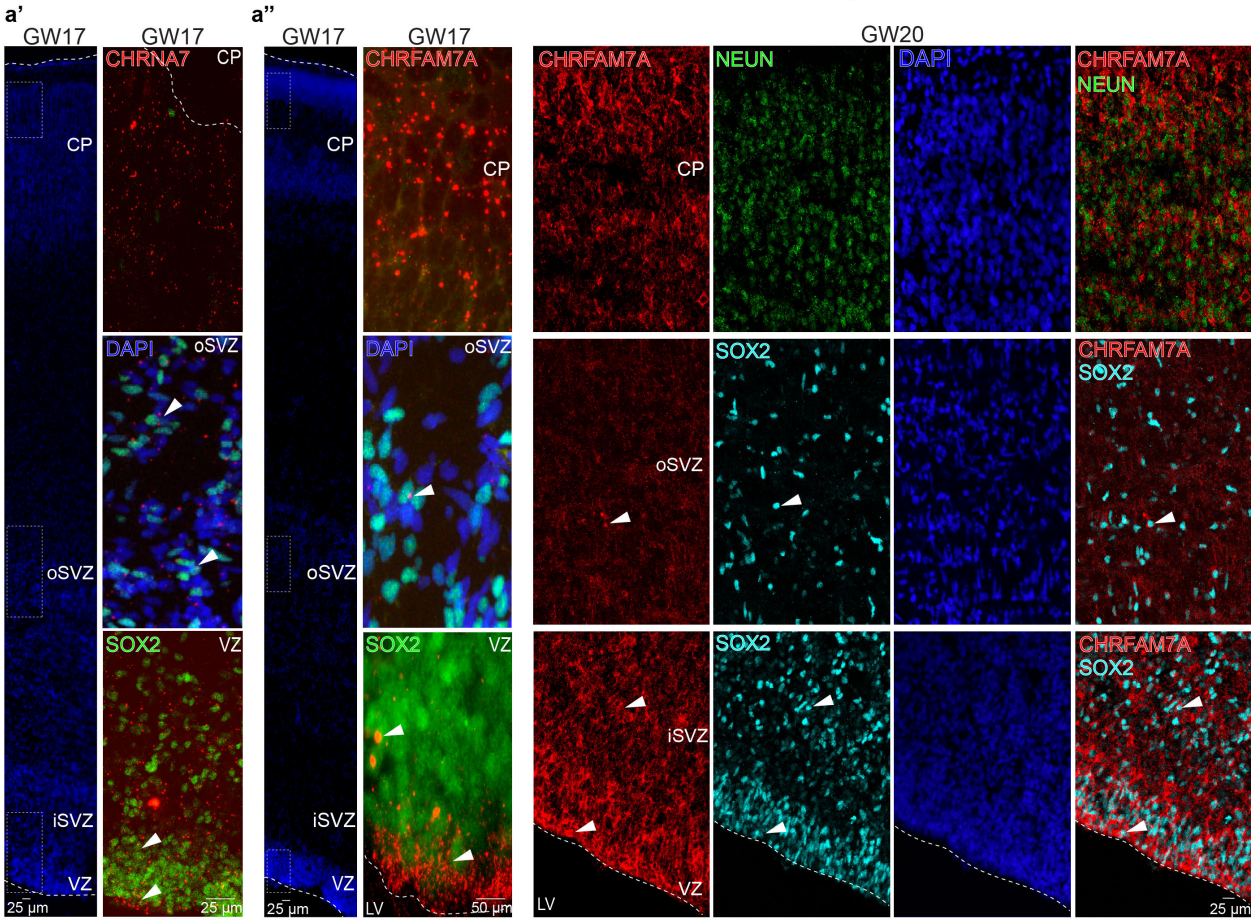

b CHRNA7 protein is expressed in the human cortex

b' CHRNA7 protein expression in oSVZ

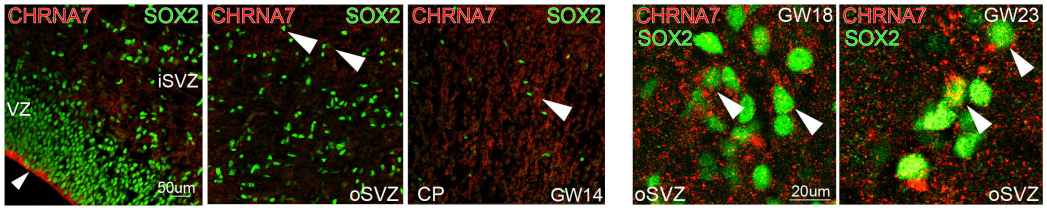

d CHRFAM7A protein is expressed in cortical organoids
Week 7-8 Cortical Organoids

e CHRFAM7A protein is expressed in late cortical organoids
Week 13-15

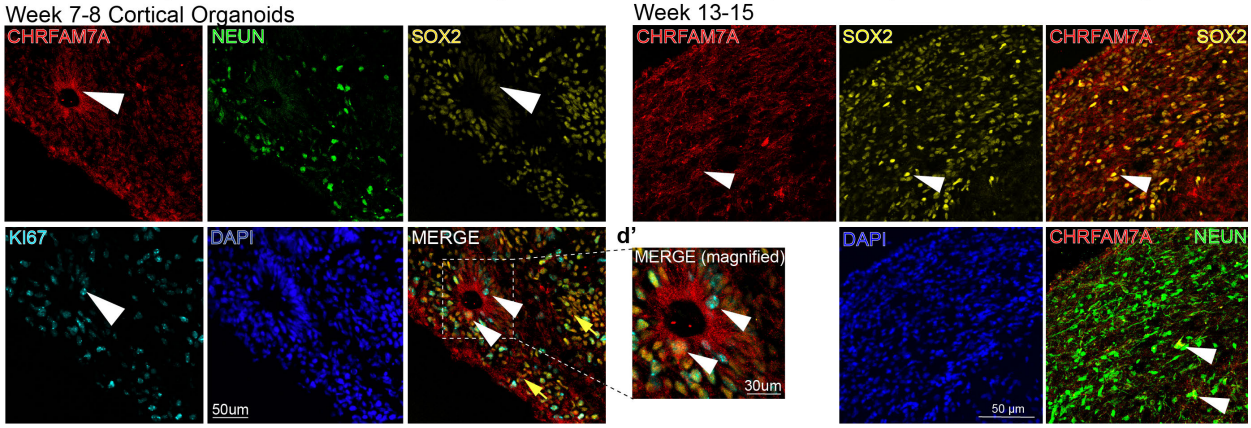

Fig. 2. Expression of Cholinergic receptor subunits CHRNA7 and CHRFAM7A in the developing cortex and cortical organoids. a, a', a''. CHRNA7 and CHRFM7A RNA expression. **a**. RNAscope for CHRNA7, and **a'**. BaseScope for CHRFAM7A, with coimmunostaining of radial glia marker SOX2 shows expression of both subunits in progenitor cells at GW17 (white arrowheads). CHRFAM7A RNA is enriched along the apical endfeet. **b,b'.** Immunostaining of CHRNA7 and SOX2, in VZ, oSVZ and CP, shown in GW14 and GW23 cortical samples **c**. Human-specific CHRFAM7A protein is enriched in the VZ. Immunostaining of CHRFAM7A validates enrichment of CHRFAM7A in the apical endfeet of the developing cortex. Colocalization of CHRFAM7A protein with SOX2 is observed in the oSVZ and VZ (white arrows). **d,d',e.** CHRFAM7A protein is expressed in ventricular RG in cerebral organoids. Immunostaining of CHRFAM7A in cortical organoids at weeks 7-9 and weeks 13-15 replicate primary tissue with expression of CHRFAM7A in SOX2+ progenitors and enrichment within neural rosettes. Abbreviations : ventricular zone (VZ), inner subventricular zone (iSVZ), outer subventricular zone (oSVZ) and Cortical plate (CP).

Fig. 3: Activation of cholinergic signaling increases progenitor cells and inhibits neuronal differentiation

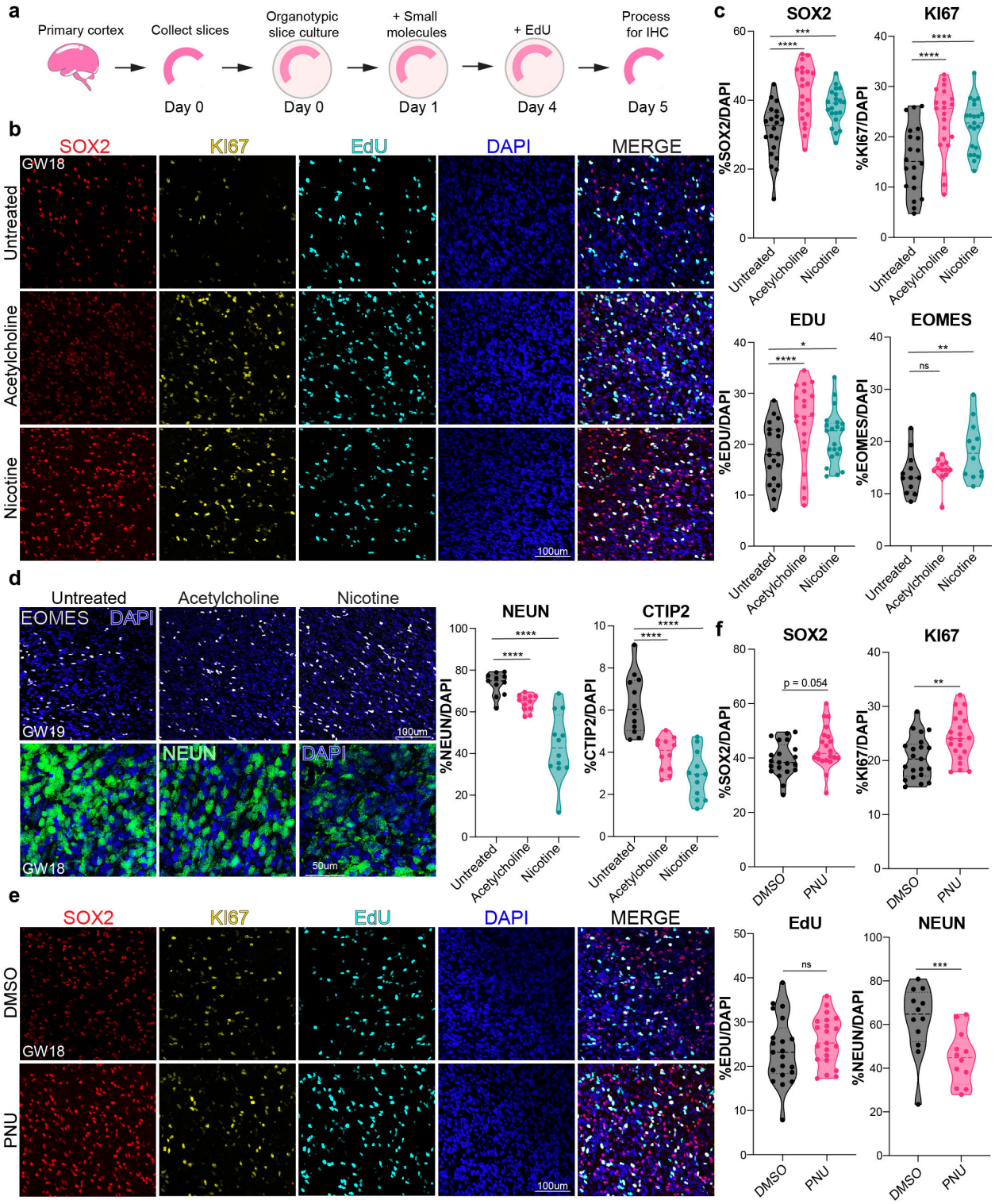

Fig. 3. Activation of cholinergic signaling in primary cortical organotypic slices by agonist treatment increases progenitor cells and inhibits neuronal differentiation. **a**. Scheme showing treatment of cortical organotypic slices with broad (ACh) and specific (nicotine, PNU) agonists for 5 consecutive days. EdU was added on Day 4 and slices fixed with 4% PFA on Day 5 for Immunohistochemistry (IHC). **b.** Representative images showing GW18 organotypic slices post ACh treatment immunostained for SOX2+, KI67+, EdU+, and co-stained with DAPI. Scale bar = 100um. **c.** Quantification of SOX2, KI67, EdU, and EOMES over total DAPI, post broad agonist treatment, n=3. Upon ACh or nicotine treatment, the number of SOX2+ progenitors increased significantly to 42.1% (p=1.12E-06), and 38.1% (p=0.0007) of DAPI+ cells respectively, compared to 30.8% in untreated (UT) control. KI67+ proliferating cells increased to 23.3% (ACh, p=1.61E-06) and 22.1% (nicotine, p=2.66E.05), compared to 15.5% in controls. We observed an increase in EdU+ cells (24% for ACh, p=8.61E-05; 21.4% for nicotine, p=0.016; 18% UT control). **d**. Representative immunostaining for EOMES and NEUN in organotypic slices treated with agonists. Scale bar = 100um. EOMES+ intermediate progenitor cells (IPCs) increased post nicotine to 18.2% (p=5.47E-05) from 13.2%, while remaining unchanged after ACh. Quantification for NEUN and CTIP2 shows changes in neuronal proportions post agonist treatment. NEUN+ neurons were reduced to 64.3% with ACh (p=0.02) and reduced to 43.5% (p=2.93E-09) with nicotine, compared to 73.4% in the UT control**.** Deep layer CTIP2+ neurons in the IZ were reduced from 6.3% to 3.9% (p=1.25E-05) with ACh, and 2.9% (p=2.14E-08) with nicotine. **e**. Immunostaining of SOX2, KI67, and EdU post PNU treatment. Scale bar = 100um. **f.** Quantification for markers post specific activation of α7 nAChR. PNU increased SOX2+ cells to 44% compared to 39% in the DMSO control, but did not reach statistical significance (p= 0.054). KI67+ cells increased to 24.2% (p=0.003) from 20.5%. PNU did not significantly impact EdU incorporation. NEUN+ neurons reduced from 63.6% in DMSO control to 45.5% (p=0.001) with PNU, (n=3), Extended datasheet 1, *p=0.05, **p=0.01, ***p=0.001, ****p=0.0001. ns= not significant.

Fig. 4: Activation of cholinergic signaling in cortical organoids shows comparable trends to primary tissue

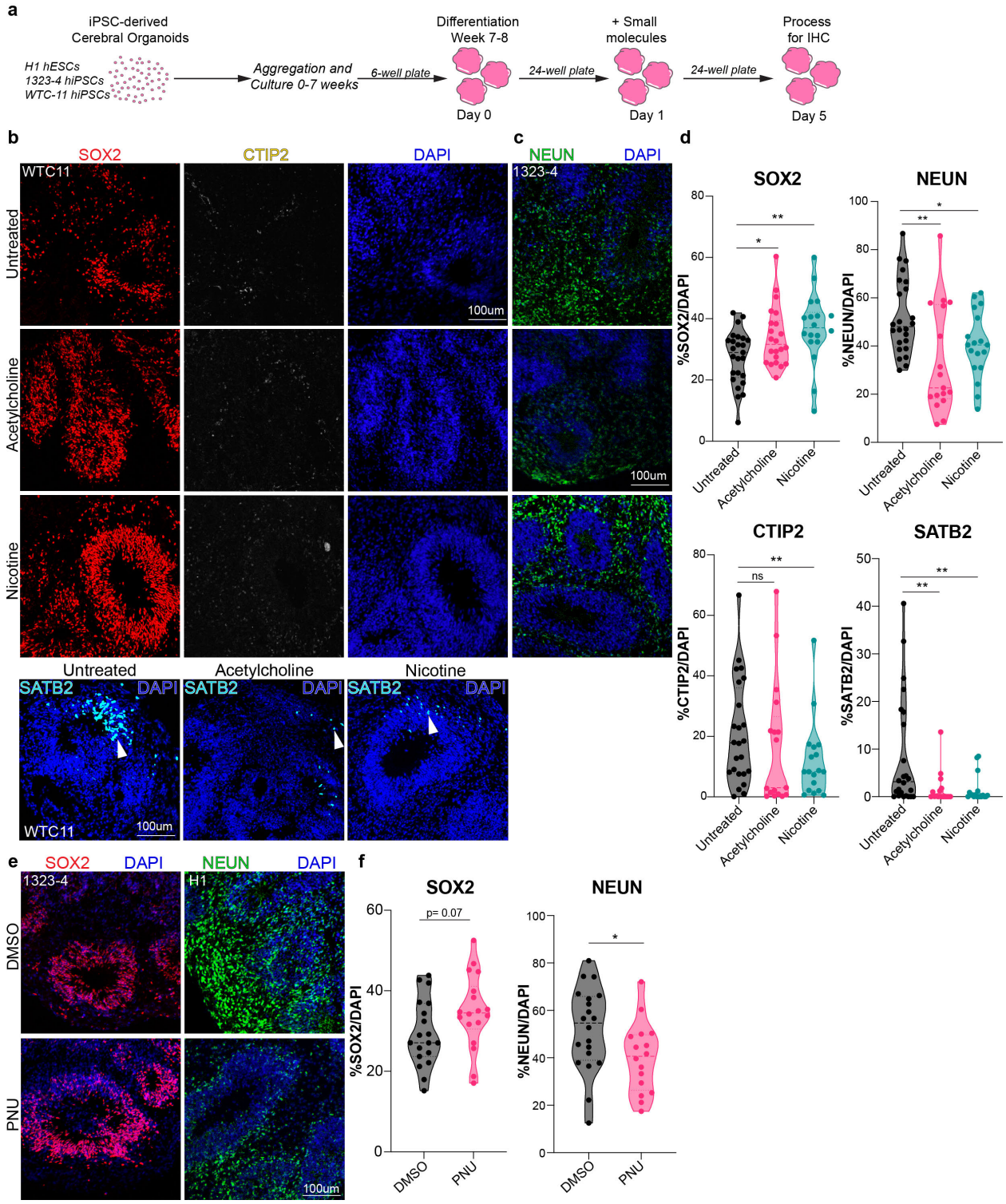

Fig. 4. **Activation of cholinergic signaling in cortical organoids shows comparable trends to primary tissue.** **a**. Scheme of cortical organoid differentiation using the Modified Sasai Protocol[1], followed by treatment with broad (ACh) and specific (nicotine, PNU) agonists. Three control cortical organoid lines were treated at differentiation Week 7-8, for 5 consecutive days, PFA fixed on Day 5 and processed for IHC. **b.** Representative images of cortical organoids, immunostained for SOX2, CTIP2 and SATB2 co-stained with DAPI. Scale bar = 100um, 50um. **c.** Representative images of cortical organoids immunostained for NEUN and co-stained with DAPI. Scale bar = 100um. **d**. Quantification for SOX2, NEUN, CTIP2 and SATB2. SOX2+ cells in ACh and nicotine increased to 37% (p=0.01) and 34% (p=0.001), respectively, compared to 27.4% in UT controls. The number of NEUN+ neurons was reduced from 52% to 34% (p=0.002) in ACh and 40.4% (p=0.02) in nicotine. SATB2+ neurons changed from 8.5% in control to 1.5% (p=0.007) and 1.4% (p=0.007) with ACh and nicotine treatment, respectively. **e.** Representative images of cortical organoids post treatment with specific agonist, PNU and DMSO control stained for SOX2, NEUN, and DAPI. Scale bar = 100um. **f.** Quantifications for SOX2 and NEUN post PNU treatment. In PNU treated organoids, SOX2+ progenitors increased from 29% in DMSO to 35% (p = 0.07) in PNU-treated conditions. NEUN+ cells were reduced to 40% (p=0.02) in PNU treated cortical organoids, compared to 52% in DMSO controls, n=3, Extended datasheet 1 , *p=0.05, **p=0.01, ***p=0.001, ****p=0.0001. ns= not significant.

Fig. 5: Loss-of-function of CHRNA7 and CHRFAM7A receptor subunits shows opposite phenotypic changes compared to cholinergic activation

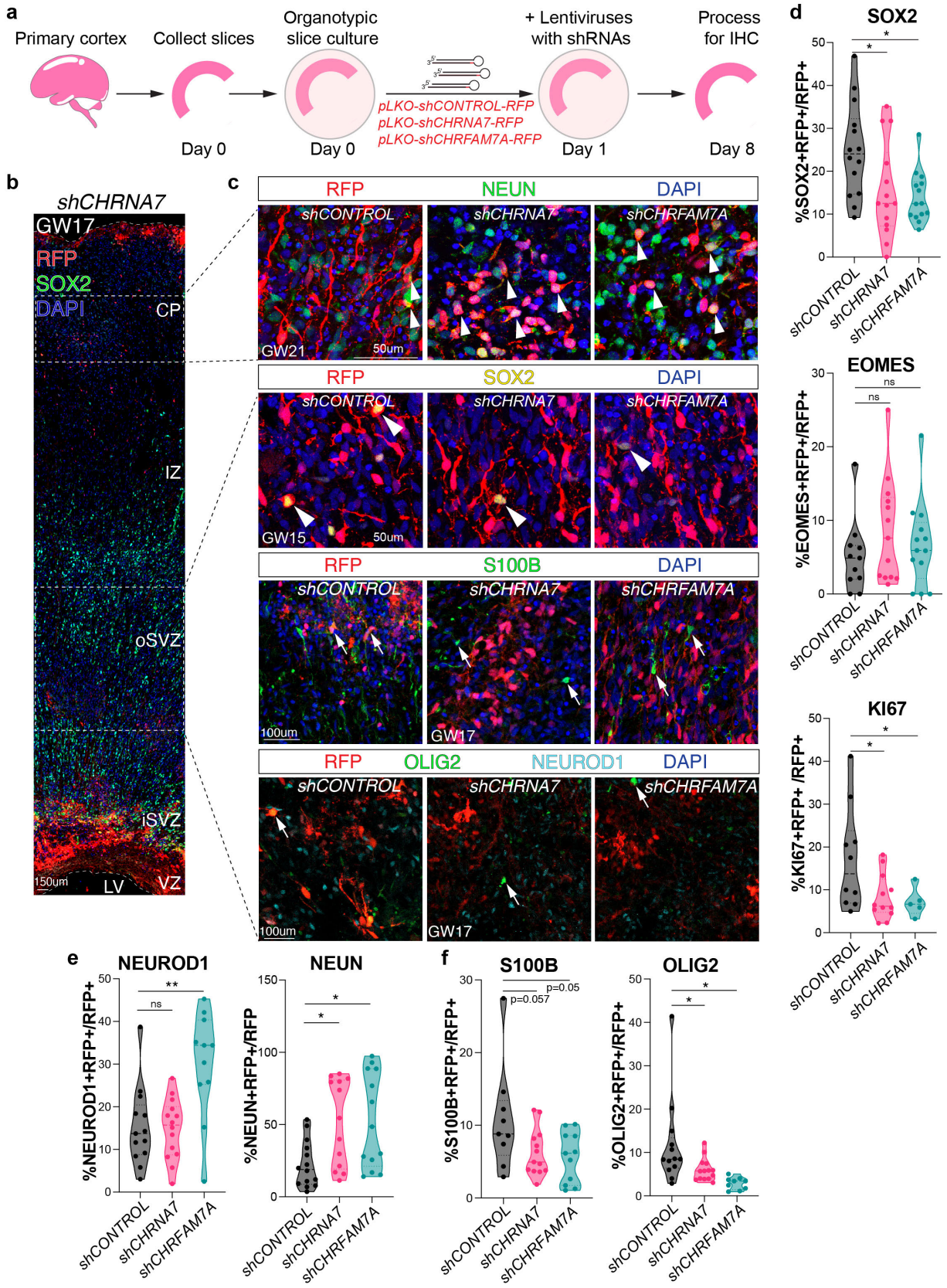

Fig. 5. **Loss-of-function of CHRNA7 and CHRFAM7A receptor subunits shows opposite phenotypic changes compared to cholinergic activation. a.** Experimental design for organotypic slice culture preparation and treatment with lentiviral mediated-shRNAs-directed against CHRNA7 or CHRFAM7A, and a scrambled control. Samples were fixed after 7-days with 4% PFA and processed for IHC. **b.** Tile scan of example shCHRNA7 sample highlighting the regions used for imaging and quantifications and **c.** Representative images of lentiviral infected, RFP+ cells, co-immunostained with NEUN+ (arrows) from GW21 with shCONTROL, shCHRNA7 and shCHRFAM7A. Scale bar = 50um. Representative images of lentiviral infected, RFP+ shCONTROL, shCHRNA7 and shCHRFAM7A cells, co-immunostained with SOX2, S100B, OLIG2 and NEUROD1 (arrowheads) at GW15 and GW17. Scale bar = 50um and 100um. **d.** Quantification of SOX2, KI67, and EOMES upon knockdown of nAChRs. SOX2+ progenitors were reduced from 25% in shCONTROL to 15.4% in shCHRNA7 (p=0.07) and 14% in shCHRFAM7A (p=0.009). KI67+ dividing progenitors were also reduced, with 8.3% in the presence of shCHRNA7 (p=0.03) and 7.1% with shCHRFAM7A (p=0.01), compared to 17% in the shCONTROL. **e.** Quantification of NEUROD1+ immature neurons upon CHRFAM7A knockdown increased from 15.3% in shCONTROL to 30% in shCHRFAM7A (p=0.0032). NEUN+ neurons upon nAChR knockdown showed the number of NEUN+ neurons increased from 22.5% in shCONTROL to 52% upon knockdown of CHRNA7 (p=0.009), and to 53% upon knockdown of CHRFAM7A (p=0.01). **f.** Quantification of S100B+ astrocytes upon AChR knockdown reduced from 11% to 6 % in shCHRNA7 (p=0.057) and to 5.5% in shCHRFAM7A (p=0.05). Quantification of OLIG2+ oligodendrocytes upon AChR knockdown reduced from 12% to 6 % in shCHRNA7 (p=0.04) and to 3% in shCHRFAM7A (p=0.01), with n=3. Extended datasheet 1, *p=0.05, **p=0.01, ns= not significant.

Fig. 6: Nicotine exposure and loss-of-function of AChRs alters Hippo signaling effectors

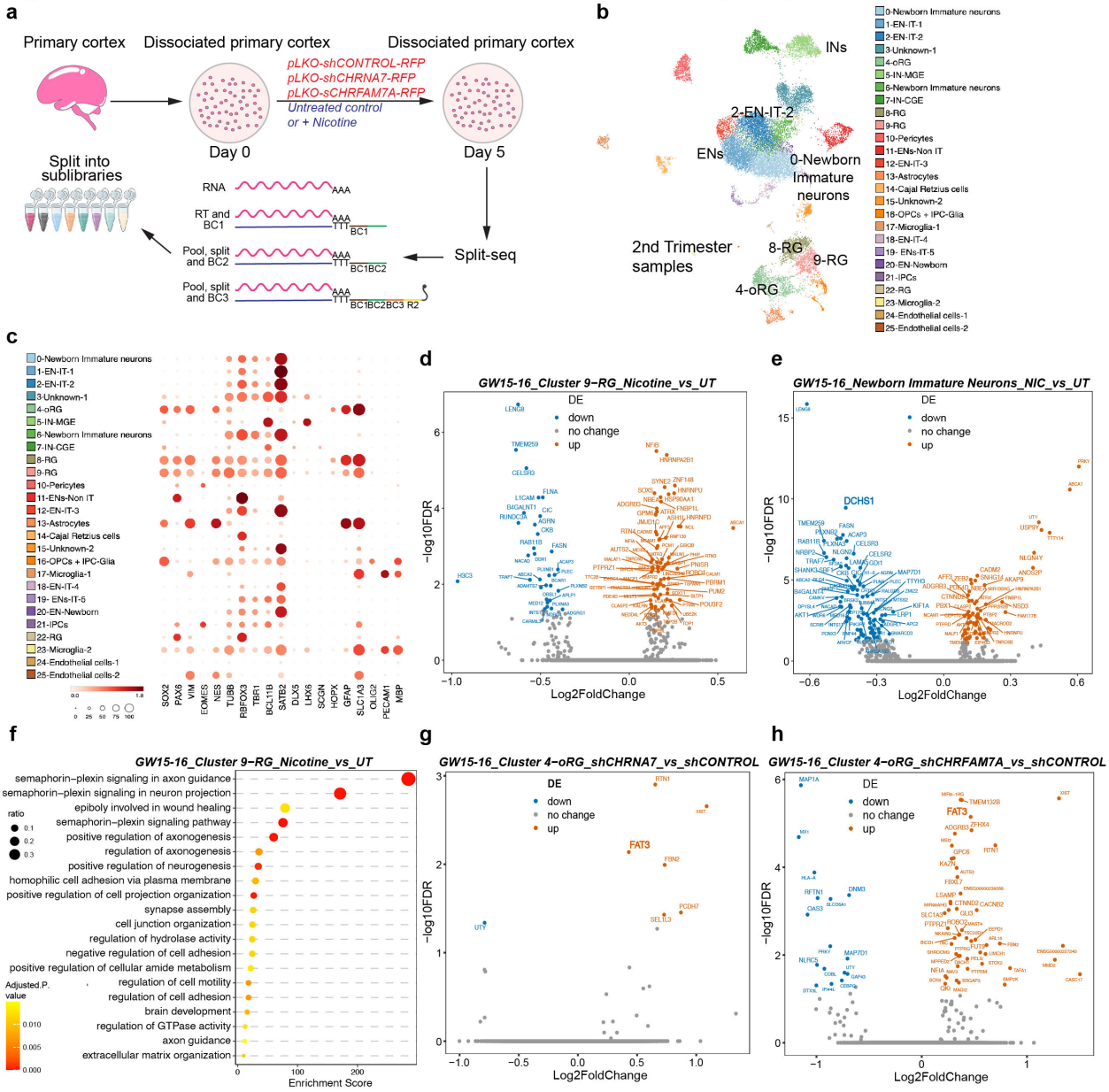

Fig. 6. Nicotine exposure and loss-of-function of AChRs alters Hippo signaling effectors. **a.** Workflow showing nicotine exposure and nAChR knockdown in primary dissociated cortical cell cultures. Cells were fixed on day 5 following the Parse Biosciences Fixation protocol and processed for Split-sequencing, a combinatorial barcoding approach where different barcodes are added in each step. We obtained 8 sublibraries. Gene expression libraries were prepared and sequenced using Illumina NovaSeq 2 Flowcell. **b.** UMAP clustering of single-cell RNA sequencing (scRNAseq) data identifies major expected cell types. **c.** scRNAseq analysis reveals anticipated patterns of marker gene expression across clusters. SOX2, PAX6, VIM, NES are expressed in radial glia and oRG clusters, while TUBB, RBFOX3, TBR1, BCL11B and SATB2 are expressed by neuronal clusters **d.** Genes up- and downregulated upon nicotine exposure in dividing neurogenic RG cells. **e.** Genes up- and downregulated upon nicotine exposure in immature neurons. One of the top downregulated genes is DCHS1, a canonical ligand of Hippo signaling. **f.** Gene Ontology (GO) for dividing neurogenic RG identifies significant pathways and processes upregulated post nicotine exposure, including Semaphorin-plexin and homophilic cell adhesion signaling. **g.** Genes up- and downregulated following knockdown of CHRNA7 in oRGs identifiies Hippo signaling receptor FAT3 among upregulated genes. **h.** Knockdown of CHRFAM7A in oRGs also identifies Hippo signaling receptor FAT3 among upregulated genes. All DEGs are listed in Extended datasheet 3.

Fig. 7: Hippo signaling effector YAP1 is downstream of cholinergic signaling

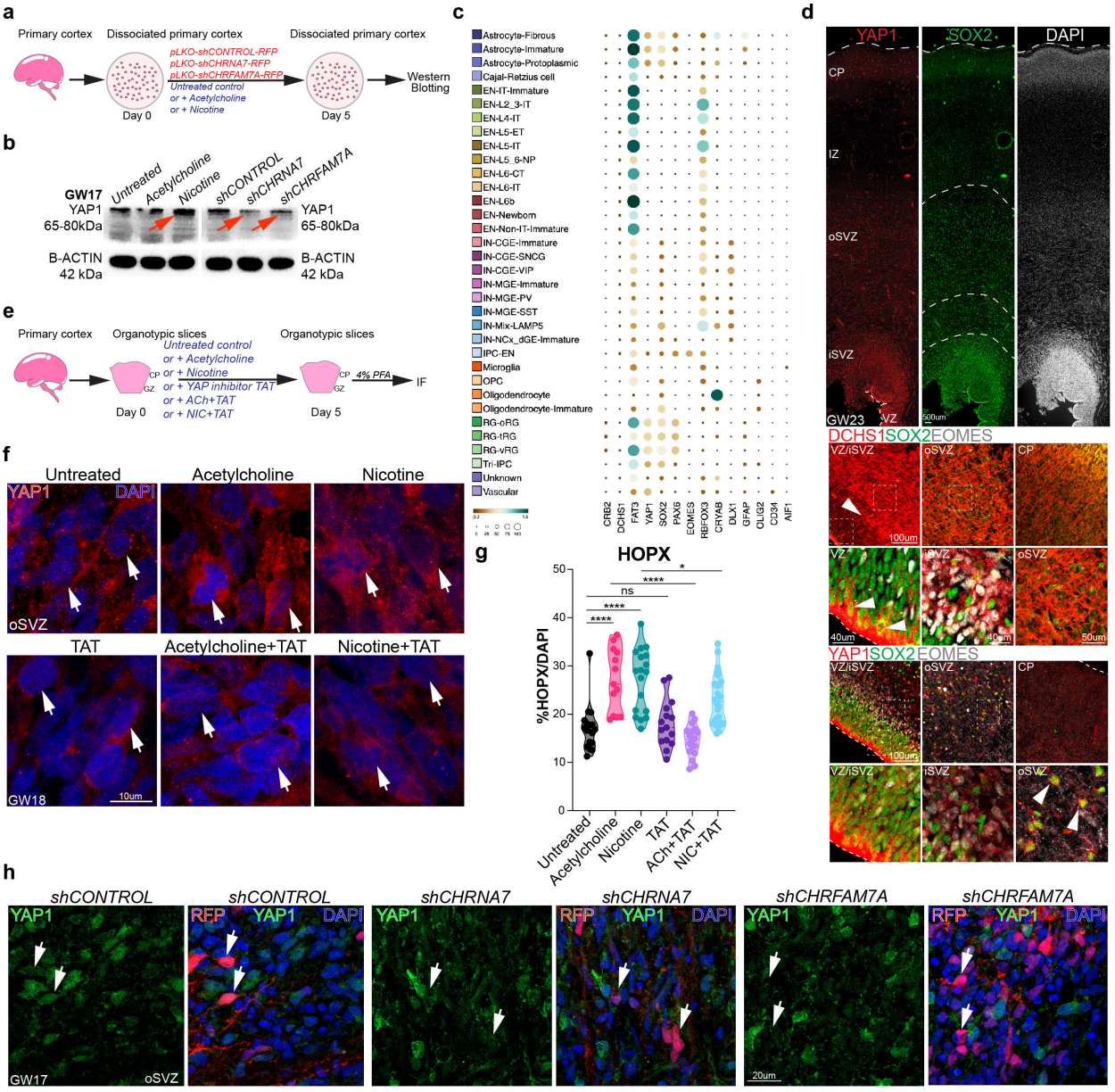

Fig. 7. Nicotine exposure and loss-of-function of AChRs alters Hippo signaling effectors. **a.** Workflow showing nicotine exposure and nAChR knockdown in primary dissociated cortical cell cultures. Cells were fixed on day 5 following the Parse Biosciences Fixation protocol and processed for Split-sequencing, a combinatorial barcoding approach where different barcodes are added in each step. We obtained 8 sublibraries. Gene expression libraries were prepared and sequenced using Illumina NovaSeq 2 Flowcell. **b.** UMAP clustering of single-cell data identifies major expected cell types. **c.** Preliminary scRNAseq analysis reveals anticipated patterns of marker gene expression across clusters. SOX2, PAX6, VIM, NES are expressed in RG and oRG clusters, while TUBB, RBFOX3, TBR1, BCL11B and SATB2 are expressed by neuronal clusters **d.** Genes up- and downregulated upon nicotine exposure in dividing neurogenic RG. **e.** Genes up- and downregulated upon nicotine exposure in immature neurons. One of the top downregulated genes is DCHS1, a canonical ligand of Hippo signaling. **f.** Gene Ontology (GO) for dividing neurogenic RG identifies significant pathways and processes upregulated post nicotine exposure, including Semaphorin-plexin and homophilic cell adhesion signaling. **g.** Genes up- and downregulated following knockdown of CHRNA7 in oRGs identifiies Hippo signaling receptor FAT3 among upregulated genes. **h.** Knockdown of CHRFAM7A in oRGs also identifies FAT3 among upregulated genes. All DEGs are listed in Extended datasheet 3.

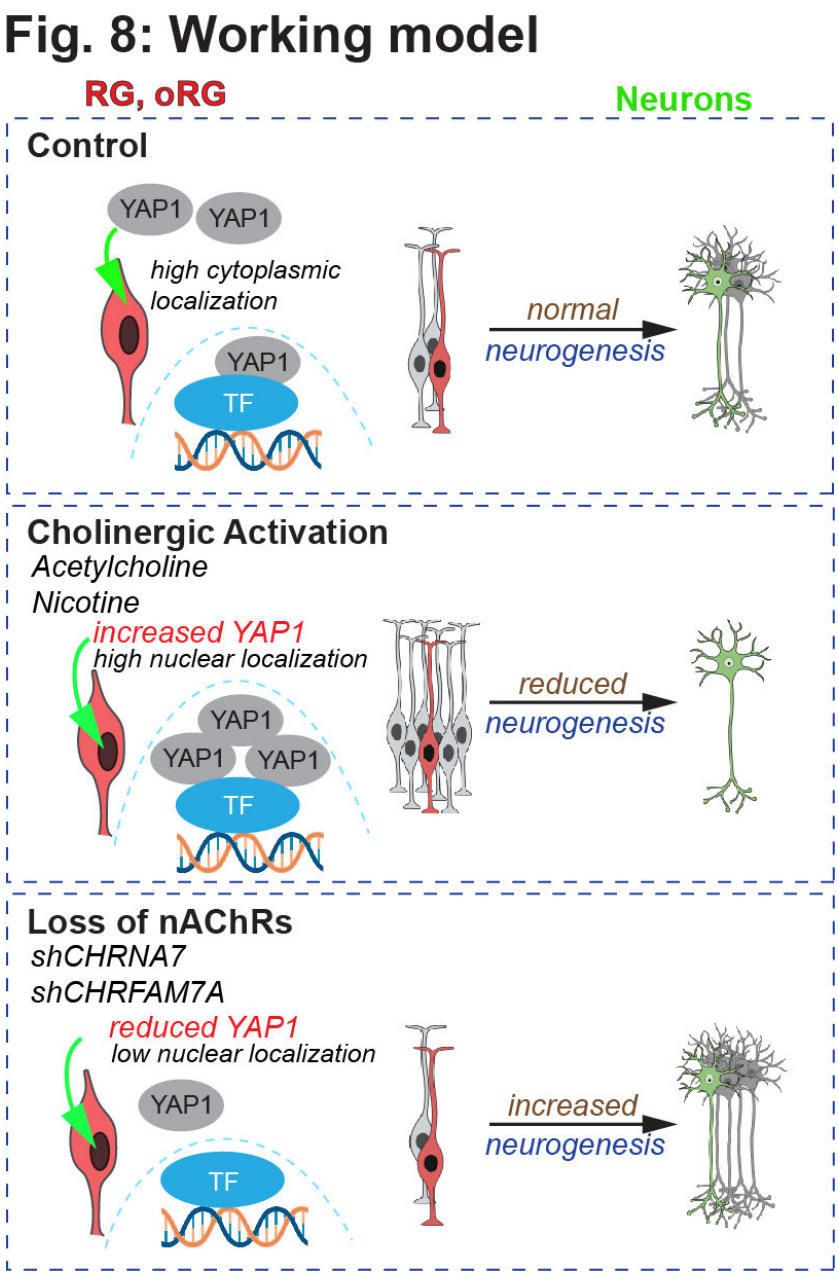

Fig. 8. Working model. Our working model proposes that nAChRs maintain a tightly regulated balance between stem cell and neurogenic fates. Agonist mediated-cholinergic activation causes a shift from neuronal differentiation towards stem cell maintenance and proliferation. The opposite is observed with knockdown of nAChRs; CHRNA7 and CHRFAM7A. These effects are partially mediated by expression and nuclear translocation of the Hippo signaling effector, Yap1. These findings highlight the essential yet underexplored role of cholinergic signaling in modulating Hippo pathway activity, influencing the fate of RG, and oRG, with potential implications for cortical development and disease.

Extended Data Fig. 1: AChE is expressed in cortical areas of the developing human brain

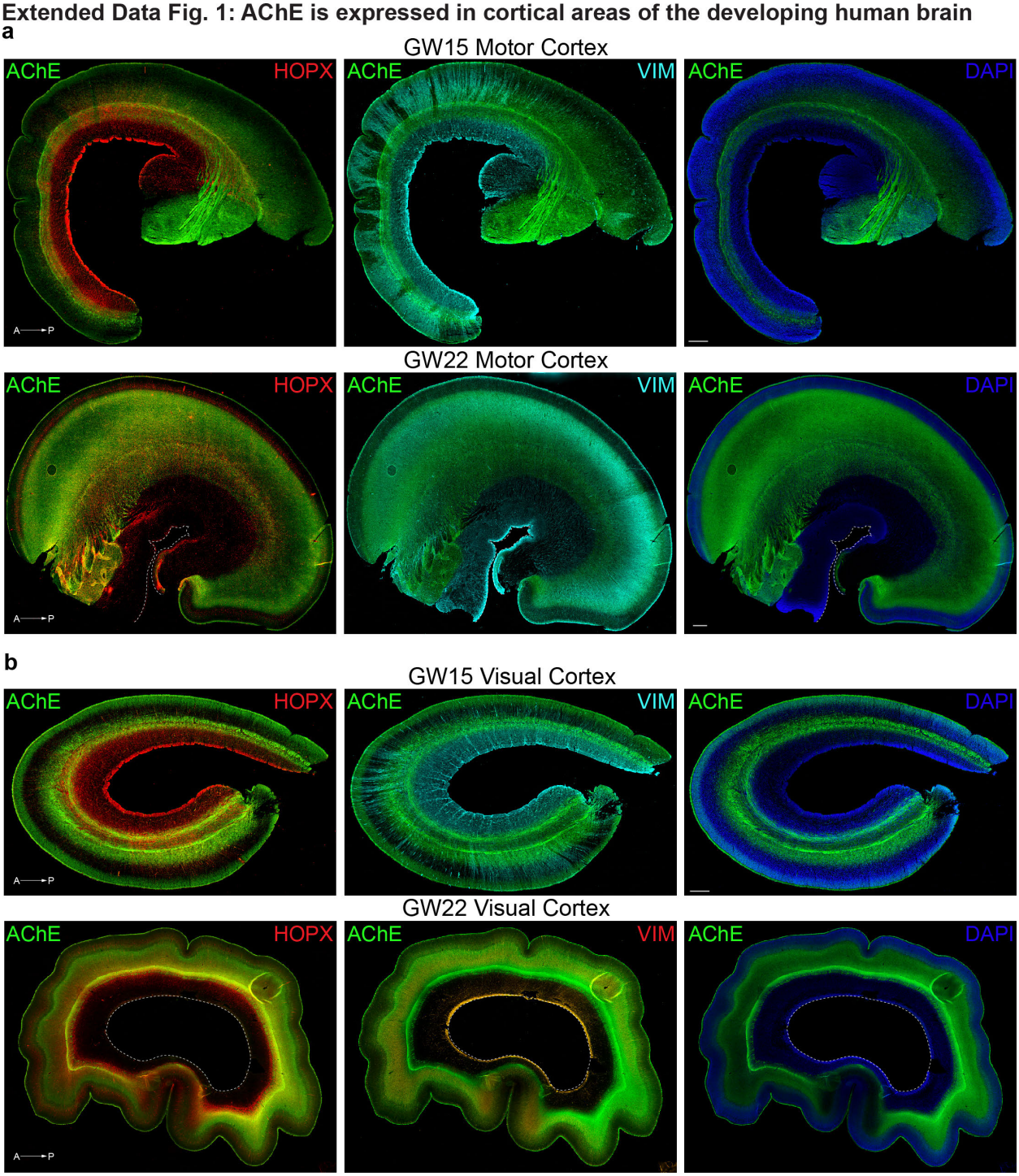

Extended Data Fig. 1. AChE is expressed in cortical areas of the developing human brain. **a.** Representative images showing immunostaining of AChE+ cholinergic fibers, HOPX+ oRG and VIM+ RG fibers at GW15 and GW22 in motor cortex. Scale bar = 500um. **b.** Representative images showing immunostaining of AChE+ cholinergic fibers, HOPX+ oRG and VIM+ RG fibers at GW15 and GW22 in visual cortex. Scale bar = 500um. Abbreviations, A-P : anterior-posterior.

Extended Data Fig. 2: Expression of nAChR receptor subunits across developing human cortex

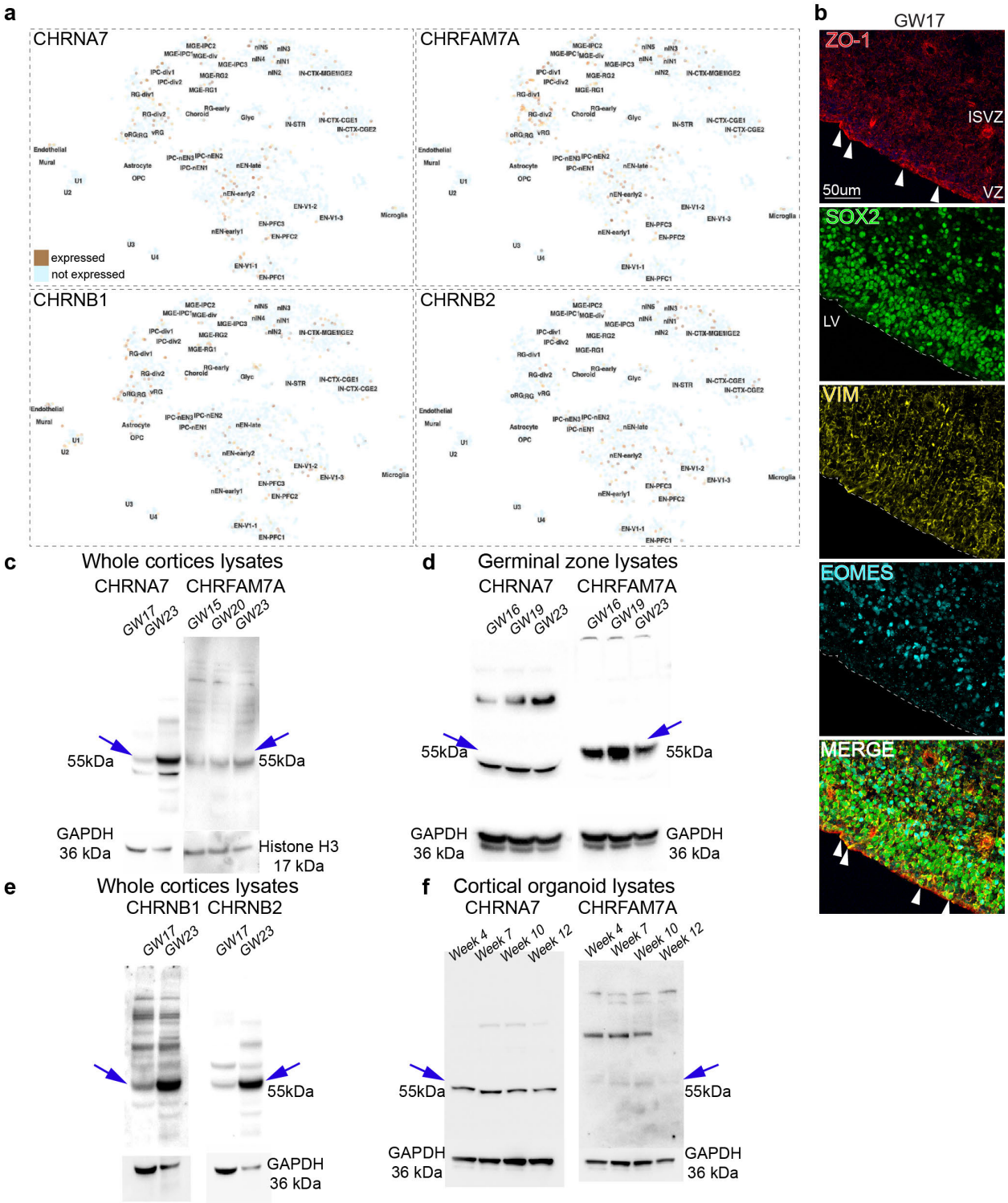

Extended Data Fig. 2. Expression of nAChR receptor subunits across developing human cortex. a. *In-silico* analysis of published single-cell sequencing data[2] shows RNA expression of

nAChR subunits CHRNA7, CHRFAM7A, CHRNB1 and CHRNB2 in the developing human cortex, including in progenitor cells. **b.** Co-immunostaining of tight junction protein 1 (ZO-1) with SOX2, VIM and EOMES showing expression in RG endfeet along the apical border of the VZ (ZO-1 staining shown by arrowheads). **c.** Western blotting confirms protein expression of CHRNA7 and CHRFAM7A across neurogenic and gliogenic time points during second trimester (n=2). **d.** Western blotting performed with protein samples enriched for germinal zone from GW16-19 shows high expression of CHRNA7 and CHRFAM7A. **e**. Western blotting for alternate nAChRs, CHRNB1 and CHRNB2, from cortical samples shows high expression of receptor subunits at GW17 and GW23. **f**. Western blotting of cortical organoids shows CHRNA7 and CHRFAM7A expression across weeks 4-12. Abbreviations : VZ : ventricular zone, iSVZ : inner subventricular zone, LV : lateral ventricle.

Extended Data Fig. 3: Expression of CHRNA7 receptor subunit across developing human cortex

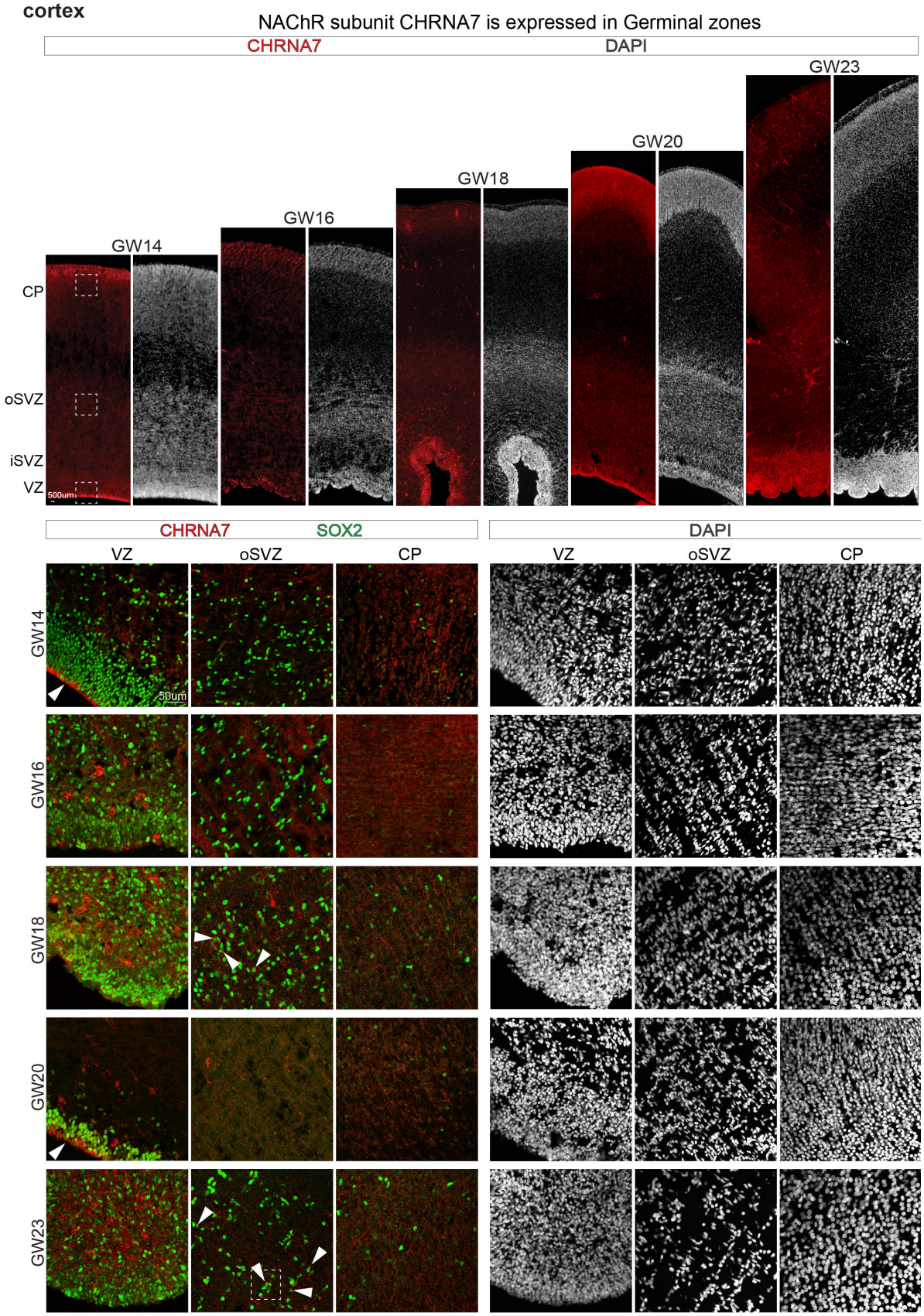

Extended Data Fig. 3. NAChR subunit CHRNA7 is expressed in germinal zones across human cortical development. Representative images from VZ to CP show co-immunostaining for CHRNA7 (nAChR), SOX2 (radial glia, outer radial glia), and DAPI (nuclei) in cortical sections from GW14, GW16, GW18, GW20, and GW23, scale bar = 500um. Magnified images highlight the expression of CHRNA7 protein (arrowheads) in the VZ, oSVZ, and CP throughout development, scale bar = 50um. VZ- Ventricular zone, iSVZ- Inner subventricular zone OSVZ- Outer subventricular zone, CP- Cortical plate.

Extended Data Fig. 4: Activation of cholinergic signaling in primary cortical organotypic slices by agonist treatment increases oRG and inhibits neuronal differentiation

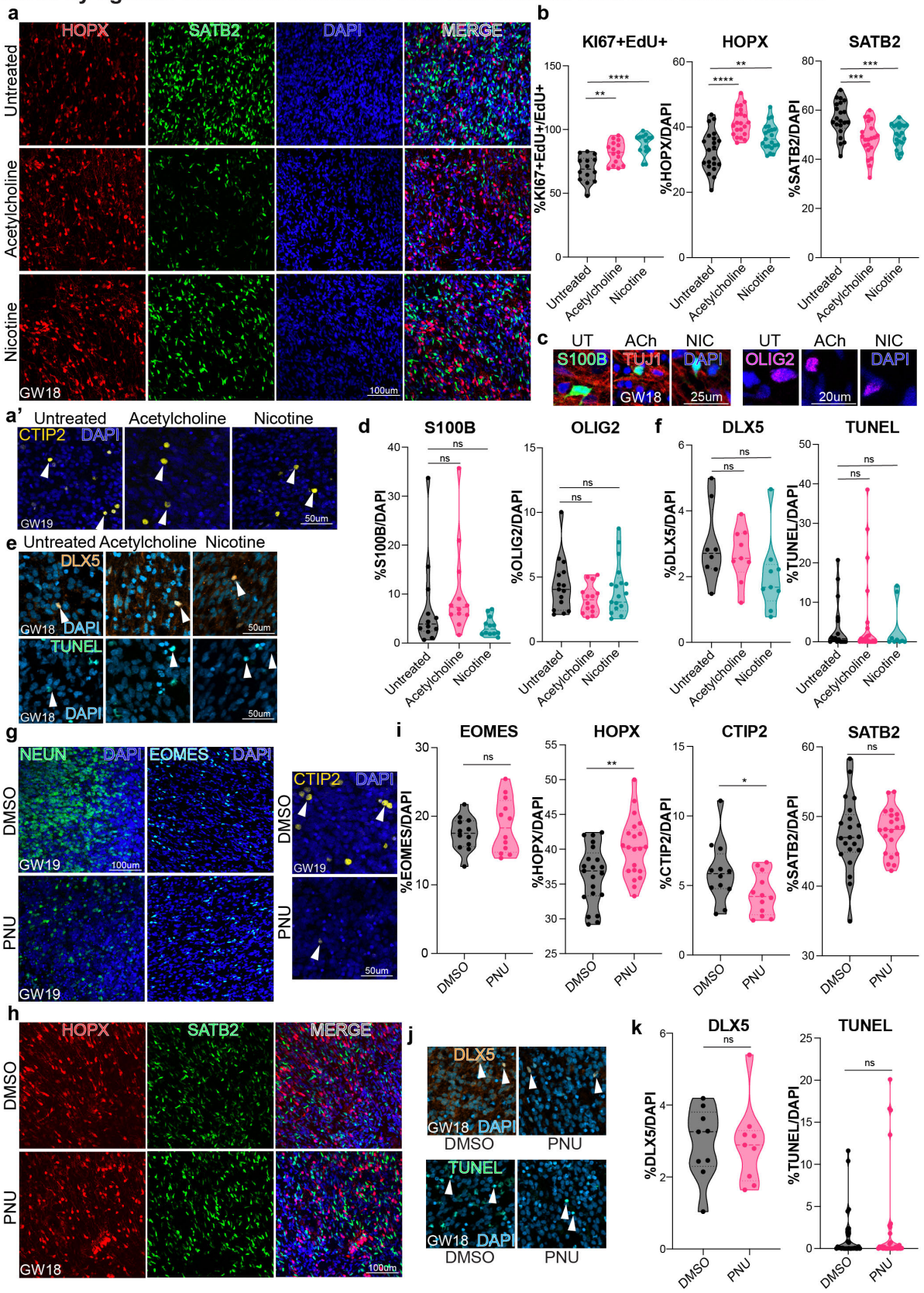

Extended Data Fig. 4. Activation of cholinergic signaling in primary cortical organotypic slices by agonist treatment increases oRGs and inhibits neuronal differentiation. **a.** Representative images showing immunostained HOPX+, SATB2+ cells co-stained with DAPI in GW18 organotypic slices, post agonist treatment. Scale bar = 100um. **a'.** Representative images of GW19 organotypic slices showing immunostained CTIP2+ cells co-stained with DAPI in the IZ post agonist treatment. Scale bar = 50um. **b.** Quantification of HOPX and SATB2 over total DAPI, post agonist treatment (n=3). We observed a significant increase in HOPX+ oRG cells with 41.5% in ACh (p=1.97E-07) and 37% (p=0.004) in nicotine, compared to 32% in control. **c.** Representative images of GW18 organotypic slices showing immunostained S100B+ and OLIG2+ cells co-stained with DAPI in the oSVZ post agonist treatments. Scale bar = 30um, 25um. **d.** Quantification of S100B and OLIG2 over total DAPI, post agonist treatment (n=3) shows no significant changes. **e.** Representative images showing immunostained DLX5+ cells and TUNEL staining in GW18 organotypic slices post agonist treatment. Scale bar = 50um. **f.** Quantification of DLX5 and TUNEL over total DAPI post agonist treatment (n=3). We observed no significant changes in DLX5 interneurons or cell death across conditions**. g,h.** Representative images showing NEUN+, EOMES+, CTIP2+, HOPX+, and SATB2+ immunostaining in GW18 and 19 organotypic slices post specific agonist treatment and DMSO control. Scale bar = 100um, and 50um for CTIP2. **i.** Quantification of cell type markers, EOMES, HOPX, CTIP2 and SATB2 in PNU-treated slice cultures compared to DMSO control. PNU did not change EOMES+ IPC numbers. HOPX+ cells increased to 40.2% (p=0.003) from 36.2% in control. We observed a reduction in neurons, impacting CTIP2+ deep layer neurons, with no change in upper layer SATB2+ neurons. **j.** Immunostaining for DLX5+ cells and TUNEL in GW18 organotypic slices post specific agonist treatment. Scale bar = 50um. **k.** Quantification for DLX5 and TUNEL over total DAPI, post specific agonist treatment showed no change (n=3), (Extended datasheet 1), *p=0.05, **p=0.01, ***p=0.001, ****p=0.0001. ns= not significant.

Extended Data Fig. 5: Activation of cholinergic signaling in early cortical organoids shows comparable trends to primary tissue

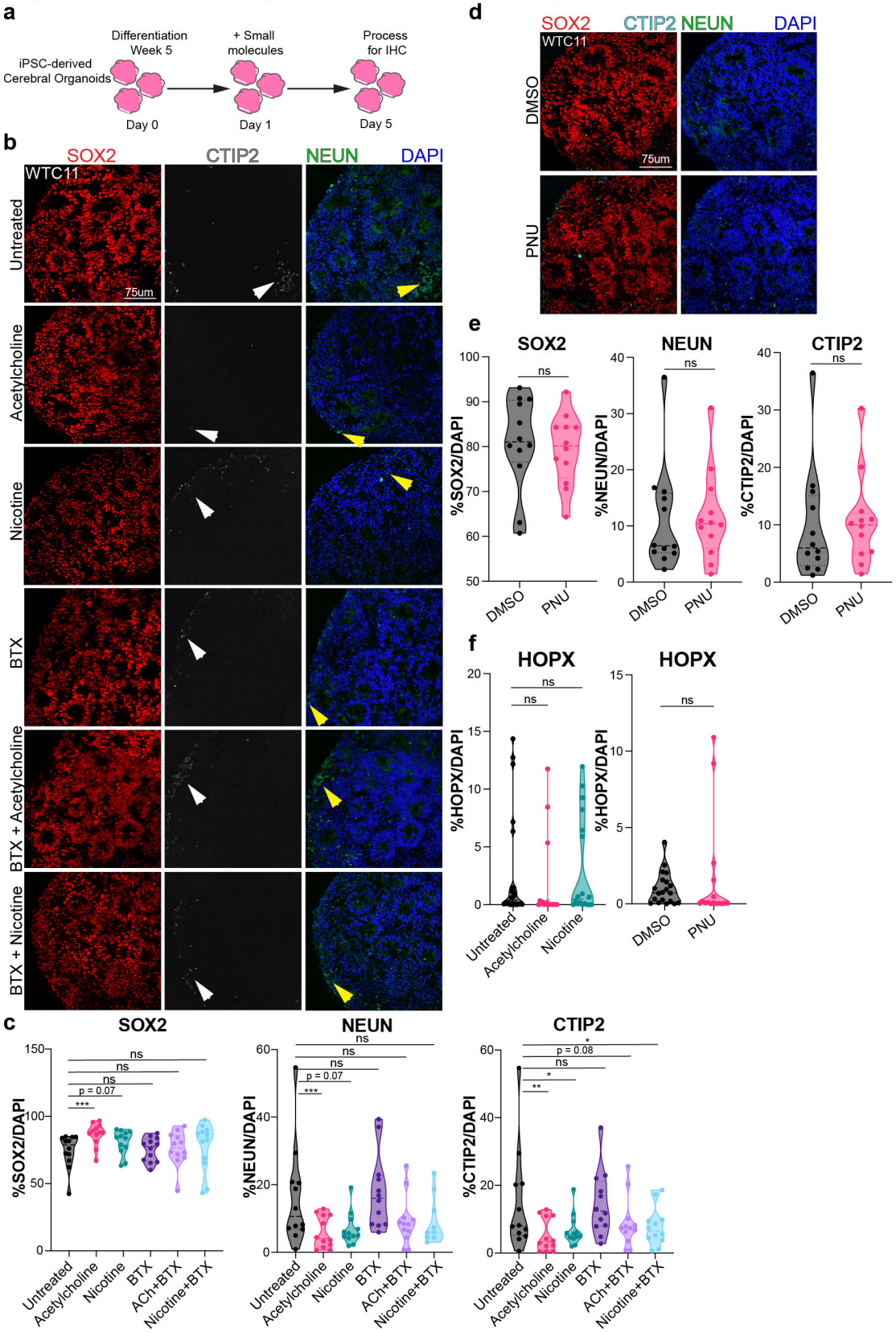

Extended Data Fig. 5. Activation of cholinergic signaling in early cortical organoids shows comparable trends to primary tissue. a. Scheme of treatment in cortical organoids with relatively broad (ACh) and specific (nicotine, PNU) agonists, the antagonist, a-bungarotoxin (BTX), and combinations of agonist + antagonist (ACh+BTX and nicotine +BTX). Three control cortical organoid lines were treated at differentiation Week 5 for five consecutive days, then PFA fixed and processed for IHC. **b.** Representative images of cortical organoids immunostained with SOX2, CTIP2 (white arrows), NEUN (yellow arrows) and DAPI. Scale bar = 75um. **c.** Quantification for SOX2, NEUN, and CTIP2 shows changes in cell types across conditions. SOX2+ progenitors increase to 86.50% (p=0.0007) with ACh and 82.31% (p=0.069) with nicotine as compared to 73.50% in control. ACh reduced NEUN+ neurons to 6% (p=0.002), and nicotine reduced them to 6.8% (0.005) from 16% in control. Similarly, CTIP2+ deep-layer neurons were reduced to 4.6% (p=0.005) and 5.6% (p=0.017) in ACh and nicotine, respectively, compared to 11.1% in control. In combination with the agonists (ACh or nicotine), the antagonist, BTX, was able to normalize the percentages of SOX2+, NEUN+ and CTIP2+ cells. BTX + ACh increased SOX2+ cells to 76.1%, while BTX+NIC increased SOX2+ cells to 77.45%, compared to 73.5% in control. We observed significant changes in NEUN+ cells, with 9.1% in BTX (p=0.03) + ACh and 8.5% in BTX + NIC (p=0.02), compared to 16.5% in UT controls. CTIP2+ cells changed slightly, with 8.8% in BTX + ACh (p=0.08) and 7.7% in BTX + nicotine (p=0.03), compared to the control with 11.1% cells. **d.** Representative images of WTC-11 cortical organoids stained for SOX2, NEUN, and DAPI, post treatment with specific agonist and DMSO control. Scale bar = 75um **e.** Quantification of SOX2 and NEUN post PNU treatment compared to DMSO control. **f.** Quantifications for HOPX+ oRG post agonist treatment show no changes (n=3) with details specified in the Extended datasheet 1, *p=0.05, **p=0.01, ***p=0.001, ****p=0.0001. ns= not significant.

Extended Data Fig. 6: Bulk RNA-seq reveals key molecular changes post CHRNA7 and CHRFAM7A knockdown

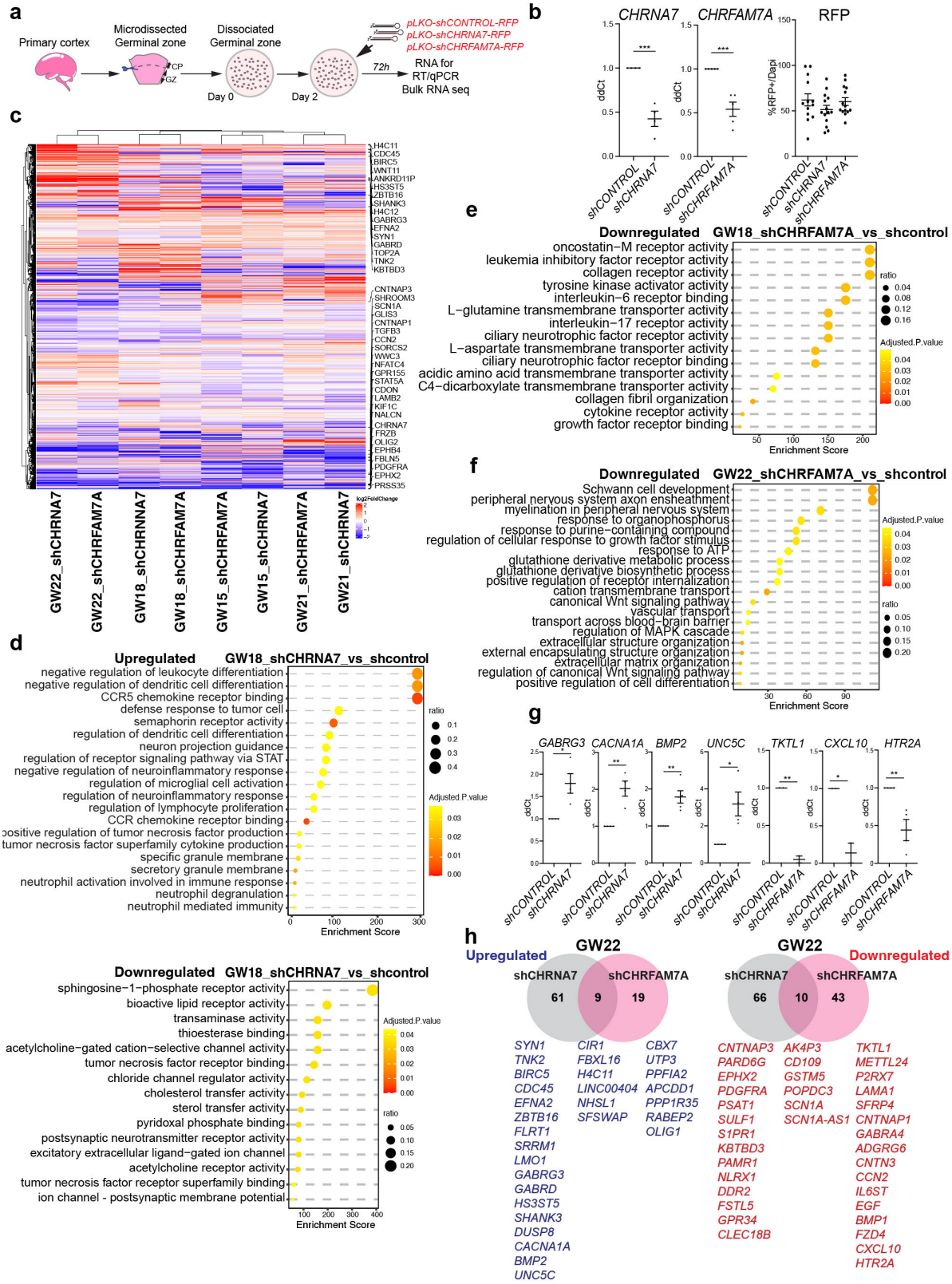

Extended Data Fig. 6. Bulk RNA-seq reveals key molecular changes post CHRNA7 and CHRFAM7A knockdown. a. Experimental design for bulk-RNA sequencing. Micro-dissected germinal zone (GZ) tissue was dissociated into adherent neural cultures and treated with lentiviral vectors carrying shRNA, directed against nAChRs and a Scrambled control. Cells were collected on Day 5 in culture, total RNA extracted and processed for Bulk-RNA-sequencing. RNA samples were tested for integrity using a BioAnalyzer. Only samples with a RIN score > 9.0 were sent for Bulk-RNA sequencing. **b.** RT/qPCR shows knockdown efficiency of receptor subunits after shRNA treatment. Quantifications for RFP+ cells/DAPI performed in organotypic slices, show comparable infection across conditions (n=3). **c**. DEG analyses identified candidate genes up- and downregulated upon knockdown of CHRNA7, CHRFAM7A, compared to the Scrambled control. **d.** Upregulated biological processes post CHRNA7 knockdown identified functions such as semaphorin signaling, chemokine receptor pathway, and inflammation. Downregulated molecular functions post CHRNA7 knockdown include lipid metabolism and chloride and acetylcholine channel activity. **e.** CHRFAM7A knockdown identified significant signaling pathways such as LIFR and tyrosine kinase pathways at GW18. **f**. Downregulated molecular functions following shCHRFAM7A in GW22 cultures include axon ensheathment and myelination. **g.** Additional biological replicates were collected for RT-qPCR validation of Bulk-RNA sequencing data. RT-qPCR validation for bulk-RNA-seq data using independent biological replicates recapitulated up- and down-regulation trends for candidate genes. **h.** Unique and shared targets post knockdown of CHRNA7 and CHRFAM7A identify potential downstream mechanisms mediated by these receptors. Blue- upregulated, Red- Downregulated. For RT/qPCR, N = 4-5, ***p=0.001. All DEGs and qPCR data are provided in the Extended datasheet 2.

Extended Data Fig. 7: Cell type diversity across samples post knockdown and agonist treatments

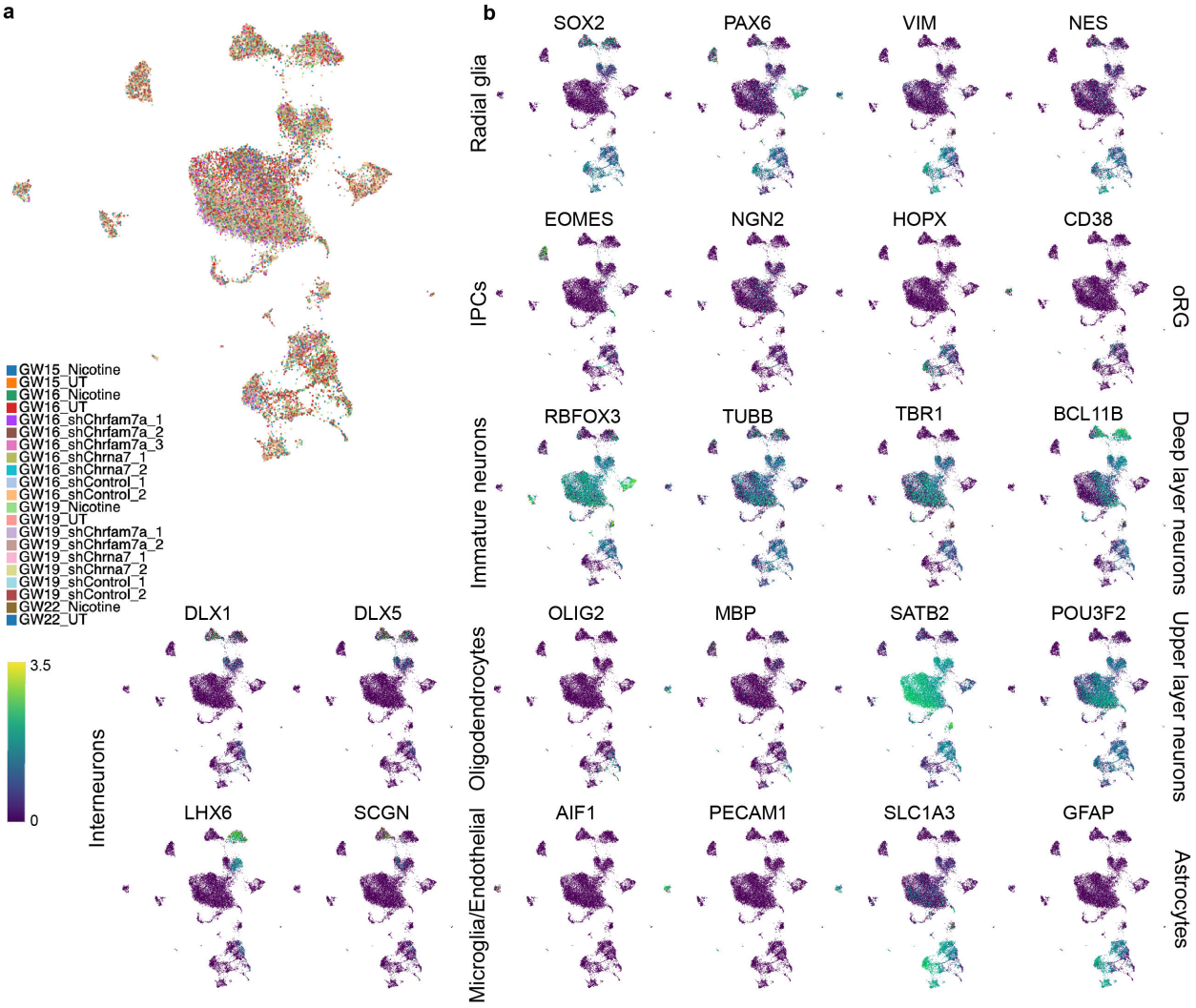

Extended Data Fig. 7. Cell type diversity across samples post knockdown and agonist treatments. a. Distribution of cell types across samples post knockdown and agonist treatments. **b.** Feature plots for known markers shows gene expression across diverse cell type clusters.

Extended Data Fig. 8. Differential Gene expression with levels of Nicotine approximating prenatal exposure

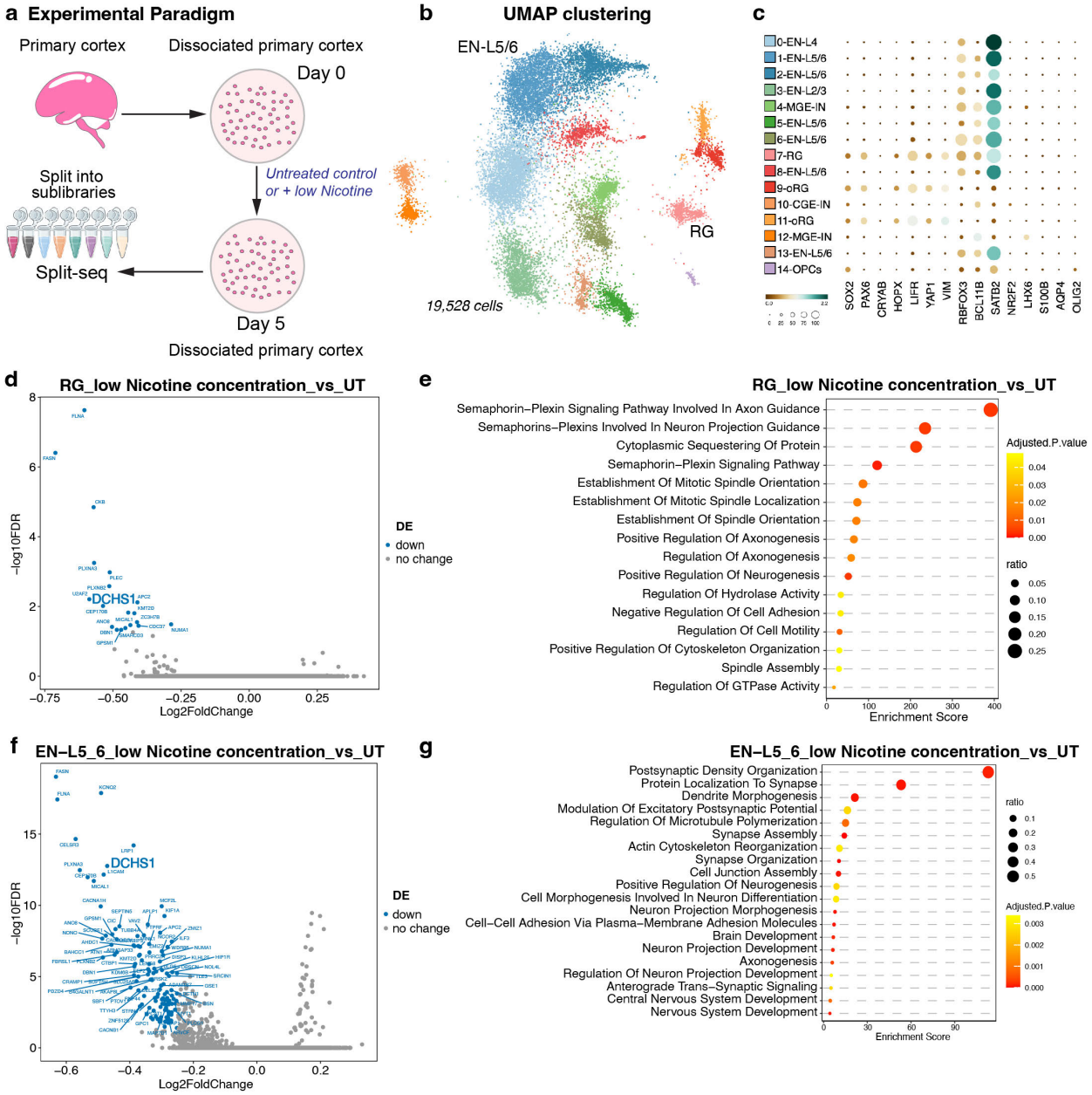

Extended Data Fig. 8. Differential gene expression with levels of Nicotine approximating fetal exposure. a. Workflow showing nicotine exposure in primary dissociated cortical cell cultures. Cells were fixed on day 5 following the Parse Biosciences Fixation protocol and processed for Split-sequencing, a combinatorial barcoding approach where different barcodes are added in each step. Gene expression libraries were prepared and sequenced using Illumina NovaSeq2 Flow cell. **b.** UMAP clustering of single-cell data identifies expected cell types. **c.** Preliminary scRNAseq analysis reveals anticipated patterns of marker gene expression across clusters. SOX2, PAX6, CRYAB, HOPX, LIFR, YAP1, VIM are expressed in RG and oRG clusters, while RBFOX3, BCL11B and SATB2 are expressed by neuronal clusters, LHX6, NR2F2, are expressed in interneurons, S100B, AQP4 and OLIG2 in astrocytes and oligodendrocytes. **d.** Genes downregulated upon nicotine exposure in RG cells. **e.** Gene Ontology (GO) for dividing RG identifies significant pathways and processes upregulated post nicotine exposure, including Semaphorin-plexin and cell adhesion signaling. **f.** Genes downregulated upon nicotine exposure in Layer 4/5 excitatory neurons. One of the top downregulated genes is *DCHS1*, a canonical ligand of Hippo signaling. **g.** Gene Ontology (GO) for Layer 4/5 excitatory neurons identifies significant pathways and processes upregulated post nicotine exposure, including postsynaptic density organization, microtubule organization, and synapse development. All DEGs are listed in Extended datasheet 3.

Extended Data Fig. 9: GO analysis post knockdown of nAChRs identifies key processes during neurogenic and gliogenic time points

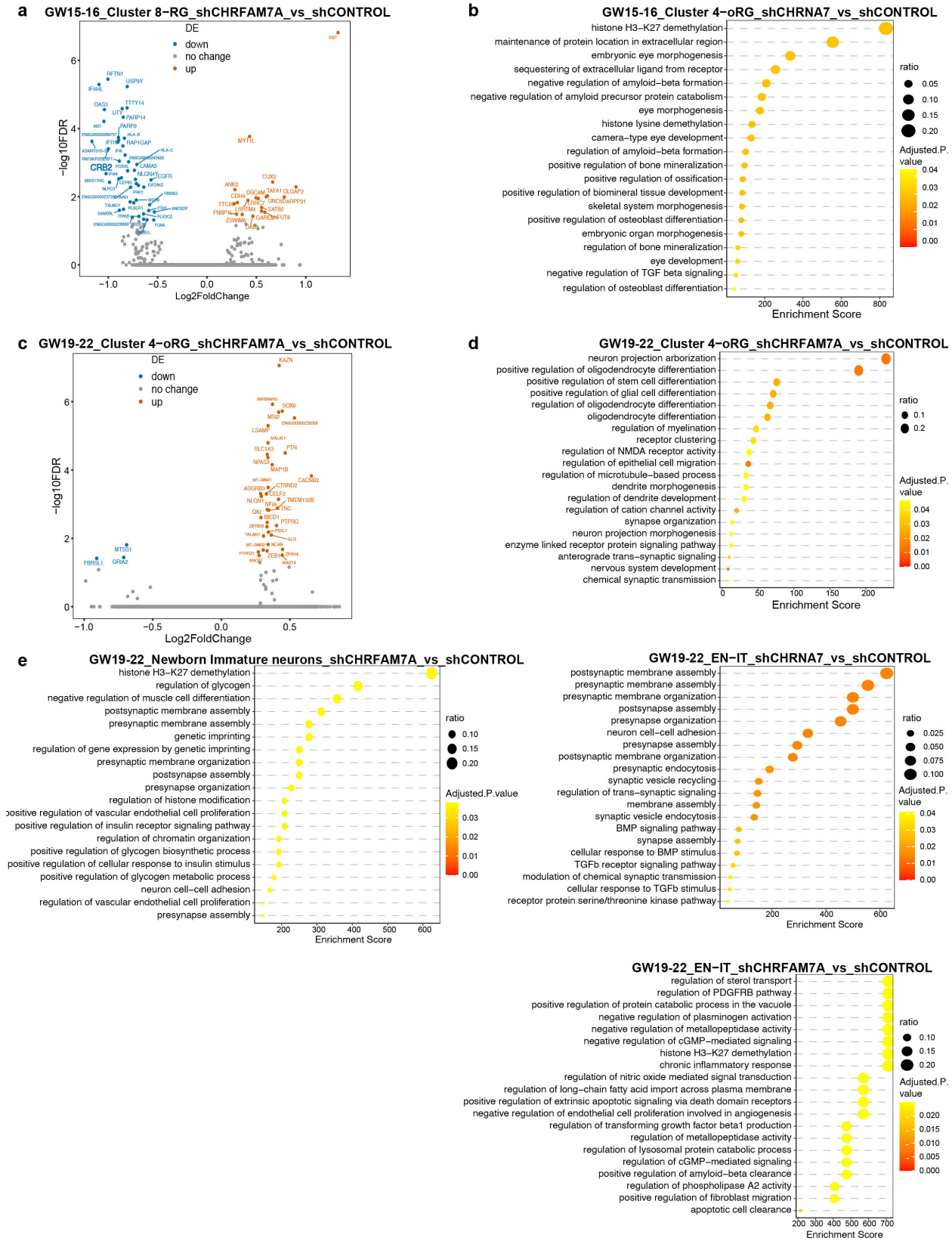

Extended Data Fig. 9. GO analysis post knockdown of nAChRs identifies key processes during gliogenic time points. a. DEGs in RG from GW15-16 after knockdown of CHRFAM7A. We observed an upregulation of MYT1L, ANK2, DLGAP2, ARPP21, DAB1, LRRC7 and upper layer neuron markers CUX2 and SATB2, while LAMA5, PODXL, WDR6, RBMS3, RFTN1, EBF1, CRB2, EGFR were downregulated in neurogenic RG. The associated GO processes in gliogenic RG post knockdown of CHRFAM7A, include, poly-D-ribosylation, cytokine-mediated signaling and axon guidance, morphogenesis of cell epithelium, integrin signaling, and ECM structural organization (Extended datasheet 3). The temporal shifts likely highlight differences in downstream molecular pathways between neurogenic and gliogenic RG mediated by CHRFAM7A. **b** GO analysis of neurogenic oRGs after knockdown of CHRNA7 impacts histone H3-K27 demethylation. **c**. DEGs in oRGs from GW19-22, after knockdown of CHRFAM7A. Knockdown of CHRFAM7A in GW19-23 oRGs led to upregulation of key genes including CACNB2, FBXL7, MAP1B, SLC1A3, NLGN1, TNC, NFIA, PTN, CTNND2 and downregulation of GRIA2, MTSS1 and FBRSL1. SLC1A3, TNC and PTN are known markers of progenitor cells and are highly expressed in oRGs[3]. MAP1B is expressed early in the developing brain and involved in axonal elongation and guidance and neuronal migration[4-8]. CTNND2 interacts with cell-cell junction proteins (cadherins), is involved in cell adhesion and synapses, and has been associated with a variety of neuropsychiatric diseases[9-11]. GRIA2 codes for glutamate AMPA receptor 2, gating an ion channel that mediates fast excitatory synaptic transmission[12]. Other associated GO processes after CHRFAM7A knockdown include oligodendrocyte differentiation, stem and glial differentiation, and myelination, processes not observed at GW15 and active at later developmental stages. **d.** GO analysis of oRG after knockdown of CHRFAM7A identifies functions related to neuron projection and glial cell differentiation. All DEGs and GO are provided in the Extended datasheet 3. **e.** GO analysis of gliogenic immature neurons includes histone H3-K27 demethylation and glycogen regulation apart from pre- and postsynaptic regulation. **f.** GO analysis of gliogenic upper layer neurons shows postsynaptic membrane assembly and BMP signaling as significant processes post knockdown of CHRNA7. **g.** GO analysis of gliogenic upper layer neurons post knockdown of CHRFAM7A shows sterol transport and PDGFR-b pathway as significant processes. All DEGs and GO are provided in the Extended datasheet 3.

References

1 Bhaduri, A. *et al.* Cell stress in cortical organoids impairs molecular subtype specification. *Nature* **578**, 142-148, doi:10.1038/s41586-020-1962-0 (2020).

2 Nowakowski, T. J. *et al.* Spatiotemporal gene expression trajectories reveal developmental hierarchies of the human cortex. *Science* **358**, 1318-1323, doi:10.1126/science.aap8809 (2017).

3 Pollen, A. A. *et al.* Molecular identity of human outer radial glia during cortical development. *Cell* **163**, 55-67, doi:10.1016/j.cell.2015.09.004 (2015).

4 Tucker, R. P., Garner, C. C. & Matus, A. In situ localization of microtubule-associated protein mRNA in the developing and adult rat brain. *Neuron* **2**, 1245-1256, doi:10.1016/0896-6273(89)90309-7 (1989).

5 Brugg, B., Reddy, D. & Matus, A. Attenuation of microtubule-associated protein 1B expression by antisense oligodeoxynucleotides inhibits initiation of neurite outgrowth. *Neuroscience* **52**, 489-496, doi:10.1016/0306-4522(93)90401-z (1993).

6 Del Rio, J. A. *et al.* MAP1B is required for Netrin 1 signaling in neuronal migration and axonal guidance. *Curr Biol* **14**, 840-850, doi:10.1016/j.cub.2004.04.046 (2004).

7 Gonzalez-Billault, C. *et al.* A role of MAP1B in Reelin-dependent neuronal migration. *Cereb Cortex* **15**, 1134-1145, doi:10.1093/cercor/bhh213 (2005).

8 Villarroel-Campos, D. & Gonzalez-Billault, C. The MAP1B case: an old MAP that is new again. *Dev Neurobiol* **74**, 953-971, doi:10.1002/dneu.22178 (2014).

9 Lu, Q. *et al.* delta-catenin, an adhesive junction-associated protein which promotes cell scattering. *J Cell Biol* **144**, 519-532, doi:10.1083/jcb.144.3.519 (1999).

10 Israely, I. *et al.* Deletion of the neuron-specific protein delta-catenin leads to severe cognitive and synaptic dysfunction. *Curr Biol* **14**, 1657-1663, doi:10.1016/j.cub.2004.08.065 (2004).

11 Lu, Q., Aguilar, B. J., Li, M., Jiang, Y. & Chen, Y. H. Genetic alterations of delta-catenin/NPRAP/Neurojungin (CTNND2): functional implications in complex human diseases. *Hum Genet* **135**, 1107-1116, doi:10.1007/s00439-016-1705-3 (2016).

12 Diering, G. H. & Huganir, R. L. The AMPA Receptor Code of Synaptic Plasticity. *Neuron* **100**, 314-329, doi:10.1016/j.neuron.2018.10.018 (2018).